ELSEVIER

Contents lists available at ScienceDirect

Environmental Challenges

journal homepage: www.elsevier.com/locate/envc



Material properties and environmental potential of developing world-derived biochar made from common crop residues



Nathan Howell*, Andy Pimentel, Sanjoy Bhattacharia

College of engineering, West Texas A&M University, Canyon 79016, TX, USA

ARTICLE INFO

Keywords: Biochar Top-Lit Updraft (tlud) Crop waste Isotherm Methyl orange developing world

ABSTRACT

Biochar is frequently made using high-tech, high-control methods which will no doubt better optimize the final material for its intended purpose and increase its value. In contrast, we used low-tech, low-control methods to produce a developing world biochar (DWB) from two common crop wastes, cottonseed (CS) and pecan shell (PS). We created DWB biochar using a top-lit updraft microgasifier (TLUD) made from paint cans, and compared it to a biochar created in a muffle furnace held at 450 °C (MF450). We first used modern material characterization methods (yield, BET, SEM/EDS, TGA, XRD, FTIR) to understand the difference in biochar production methods on the feedstock. We then used batch equilibrium adsorption with cationic and anionic dyes (methyl orange, MO and crystal violet, CV) to examine environmental performance. The TLUD method generally has a lower biochar production yield than MF450 because we believe much of the material in the TLUD achieves temperatures > 450 °C and is sometimes difficult to retain in the device. The higher temperatures in the TLUD device lead to a biochar which is more microporous, has greater surface area, has less surface functional groups, has greater ash content, is more carbonized, and has lower residual cellulose crystallinity.

There were differences in adsorption performance whereby the MF450 biochar adsorbs CV more strongly than the TLUD. For MO, PS-TLUD is less effective at adsorbing the dye when compared to PS-MF450, while CS-TLUD has a much higher adsorption strength than CS-MF450. We are not certain why the two methods show opposite effects in different feedstock but speculate that it may have to do with the much higher mineral content in the PS-TLUD compared to its MF450 counterpart. Out of many isotherms examined Freundlich and Langmuir isotherms provide a best-fit to our data only about half the time. Sometimes an S-shaped isotherm was the best fit or still fit the data reasonably well. Comparing the dye adsorption to other studies, the DWB does not adsorb as well, yet it is still effective for removal at environmental dye concentrations of relevance. Overall, we conclude that DWB, made in this uncontrolled fashion, can make a reasonably high quality biochar based on material properties and environmental performance. We suggest that additional research be done on other low-tech biochar production methods to see how to scale-up and optimize them according a developing world community's intended use.

1. Introduction

Biochar is generally defined as any pyrolyzed high carbon mass heated under limited oxygen conditions. It has been made from many types of crop residue (Gai et al., 2014; Kang et al., 2018; Lee et al., 2010; Mandal et al., 2017; Novak et al., 2014; Peterson and Jackson, 2014; Yu et al., 2016; Yuan and Xu, 2011; Zhang et al., 2016), animal dung(Cao et al., 2009; Cely et al., 2015; Janczak et al., 2017; Meng et al., 2013; Novak et al., 2014; Uzoma et al., 2011), excess activated sludge(de la Rosa et al., 2018; Fan et al., 2017; Mendez et al., 2012; Nansubuga et al., 2015; Paneque et al., 2016), sediment(Song et al., 2019), and waste plastics(Li et al., 2021; Noori et al., 2020; Peng et al., 2021; Rajendran et al., 2020; Ro et al., 2014; Sajdak et al., 2015; Xu et al., 2018;

Xue et al., 2015) to give just a few examples of the interest in its production. Biochar varies according to several factors, which include feedstock but also production method and conditions, post-production processing, and post-production modification (Ahmad et al., 2014; Li et al., 2019; Rajapaksha et al., 2016; Xie et al., 2015). Because biochar is made from materials that are low value or are simply considered waste, it fits into a common framework of waste-to-product transition. The proposed environmental benefits of biochar fall into four major areas, which are not mutually exclusive. Those areas are waste reduction, carbon sequestration, agricultural soil amendment, and water treatment and/or pollutant mitigation (Lehmann and Joseph, 2015).

The fact that biochar has been studied so extensively is indicative of at least two possible views on its use. The first is that biochar is highly

E-mail address: nhowell@wtamu.edu (N. Howell).

^{*} Corresponding author.

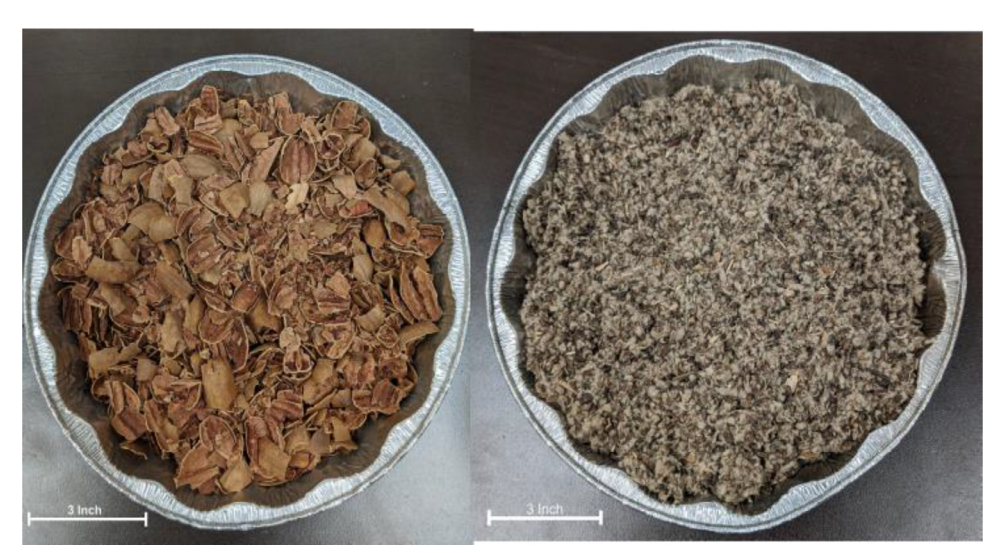


Fig. 1. Pecan shell (left) and cottonseed (right) raw biomass feedstock.

adaptable to a specific need and a specific context (Rajapaksha et al., 2016). People make biochar from most any high carbon material available in a local context, and the way that is it is produced and post-processed can make it most suitable for the intended application. A second view of biochar is its profitability as a form of waste-to-product. Because biochar is made from materials that would otherwise be considered waste and because it can be made relatively simply, there is a potential for it to be both useful and profitable. If the increased production cost of biochar is balanced by the increased quality and therefore economic return of the product, then the increased cost is justified at least on purely economic grounds. However, we would like to consider the possibility for biochar in low resource, developing world settings.

Researchers have examined what we would call developing world biochar (DWB) previously (Bayabil et al., 2015; Gwenzi et al., 2015; Kearns, 2012; Lohri et al., 2016), which we generally define as biochar produced from local waste products, using inexpensive methods and materials, and produced without extensive education in pyrolytic process design. In these settings even if the utility of biochar can be increased with more expensive and more controlled processes, these processes may not be available for any number of techno-economic or social reasons. Despite the potential for developing world communities to make and employ DWB, there are few studies specifically on this type of biochar. Many of them deal with biochar for use as a charcoal fuel and not water or agricultural benefit.

Perhaps nowhere is the value of biochar most readily clear than in developing world agriculture. Agricultural activity in developing nations is increasing as developing world population increases due to increased demands for food and fiber. The Food and Agriculture Organization of the United Nations (FAO) predicts that in the near term additional arable land will need to be opened up for rain-fed production of permanent crops. Much of this land is in tropical Latin America and Sub-Saharan Africa, places where forests are mixed with surface water and groundwater of environmental importance.(FAO, 2002) Moreover, FAO indicates that to meet world calorie supply needed for projected population growth 77% of agricultural land increases will come from developing countries (Alexandratos and Bruinsma, 2012). Therefore, we are interested in the quality of biochars that we can make from available developing world feedstock and methods.

The purpose of this study is to compare the material and agroenvironmental performance differences in biochars made by from common waste feedstock (cottonseed and pecan shell) and made by two different means—a more controlled and technologically intensive "developed world" biochar and a low resource "developing world" biochar (DWB). We intend to fill the void in understanding DWB potential through examination of DWB materially (SEM/EDS, BET, XRD, FTIR, TGA) and environmentally (use of cationic and anionic dye adsorbate models). The use of the biochar in this study is with a view predominantly towards water and wastewater treatment, but may still be relevant for agricultural and remedial applications in developing communities

2. Materials and methods

2.1. Biochar production

We chose the waste feedstock utilized in this study based on their availability and how easily they can be procured in the developing world. Both pecans and cotton are widely produced in the world due to their marketability and uses. Pecans, although endemic to the United States, have been exported and grown in various parts of the developing world. In order for the pecan nuts to reach maturity, the trees must live in an environment that allows them to have 205–233 frost-free days. This restricts pecan production to the southern states in the United States and countries such as Australia, Brazil, Israel, Mexico, Peru, and South Africa (Blayney and Gutierrez, 2017). Cotton is a common cash crop and with the existence of GMO varieties, its production has become much more prevalent in the developing world (Brookes and Barfoot, 2018). The production and use of both pecans and cotton yields waste biomass in the forms of Pecan Shell and Cottonseed (PS, CS, Fig. 1) that can be easily obtained and pyrolyzed and into biochar.

We synthesized these biochars using a Top Lit Updraft (TLUD) device that can be easily reproduced in the developing world and a muffle furnace which mimics what could be used in the developed world.

The most common, and likely most viable methods for producing DWB include mound kilns, brick kilns, open pits, and top-lit updraft micro-gasifiers (TLUD) (Lehmann and Joseph, 2015). While it is certain that these methods are used to produced biochar in developing world agricultural settings, the research on the quality of biochar produced in these settings and associated agro-environmental benefits is not nearly as extensive as for more industrially produced biochars as evidenced by the small number of studies we found.

TLUD devices are known for their low pollution emissions, efficiency, and their ability to produce syngas and synthesize biochar simultaneously (James et al., 2016). These devices are designed to intake air from underneath and allow it to flow through and release combustion exhaust from the upper chimney. This process allows the combustion layer to move through the biomass precursor from top to bottom pyrolyzing the biomass and the remaining high-carbon product is biochar (Bhadha et al., 2021; James et al., 2016). A search revealed in the Web of Science data revealed there have been only eight (8) studies which

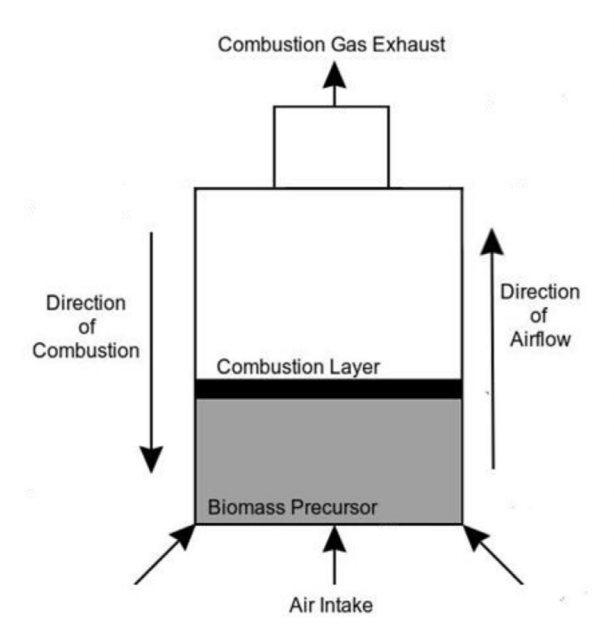




Fig. 2. Top lit updraft (TLUD) biochar production unit.

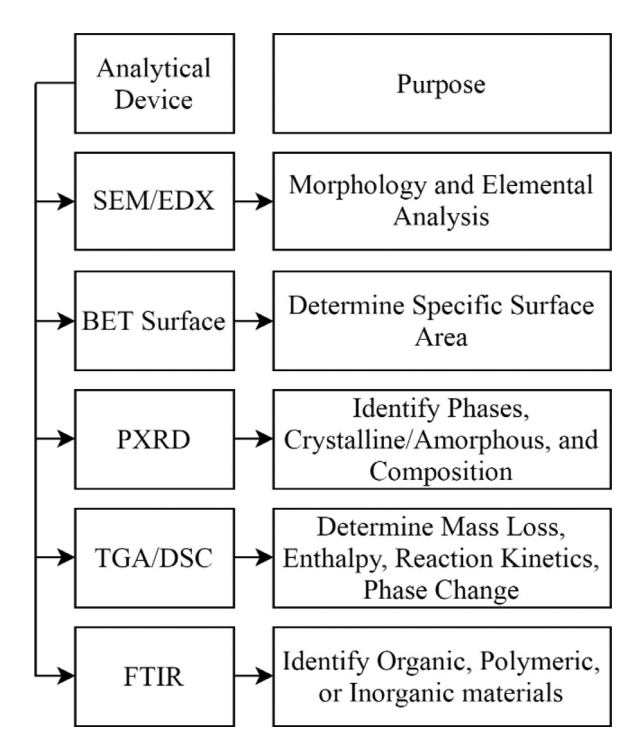


Fig. 3. Analytical Devices Used to Determine Biochar Properties.

have examined TLUDs and biochar in any way. They include studies that examine it in the low resource/low impact settings in terms of LCA impacts (Sparrevik et al., 2013), heating and cooking (Birzer et al., 2014; Deng et al., 2018; Maican et al., 2017; Tryner et al., 2014), and biochar production (Gonzaga et al., 2017; Masis-Melendez et al., 2020; Pandit et al., 2017). Fig. 2 is a representation of the process we used and our TLUD prototype.

We constructed the developing world TLUD device by easily obtained metal components such as a paint canister and a food can. We perforated the paint can along its top and bottom edges so that it contains a series of holes on its underside and a large hole in its lid. The upper can has its top and bottom removed and is placed over the hole in the lid to help direct airflow.

To utilize the device we loosely packed the biomass precursor in the paint canister. We then dowsed it with a small amount of lighter fluid and applied a flame. We covered the canister with the lid and chimney. Approximately 30–50 min are necessary for the biomass to pyrolyze completely. We ceased pyrolysis and the flame by quickly emptying the can and covering to limit oxygen while cooling.

To produce biochar in a muffle furnace, the precursor biomasses were packed into ceramic crucibles and covered to limit their exposure to oxygen. These crucibles were then placed into the furnace and pyrolyzed at 450 °C for 20–30 min depending on the biomass precursor. The exact pyrolysis time depended on the feedstock. We sought to pyrolyze the whole sample mass without extensive ashing (as observed by graying of the sample).

For both biochar production methods, we covered the hot biochar, and then allowed it to cool for 30 min-1 h. We then washed it in DI and put in a dryer at 100 °C for several hours. We crushed the resultant biochar and sieved it to retain particles approximately $< 63~\mu m$ in size (passing through no. 200 sieve).

Initially, we used five (5) waste crop residue feedstock, which we could easily procure and which are frequently available in developing world agriculture—peanut shells, rice husks, cottonseed waste, wheat straw, and coconut coir. Based on early surface area and adsorption tests, we focused our study on CS and PS, but we do present some results of these other feedstock. For all crop residues, we did not pre-process these materials in any way before pyrolysis. We pyrolyzed them "as is". We identify each biochar type according to feedstock and method production. For example, biochar made from pecan shell in the muffle furnace at 450 °C is named PS-MF450.

2.2. Material characterization

As shown in Figure 3, we employed an array of various analytical tools were employed to characterize their various properties and differences.

2.3. Sorption studies

2.3.1. Explanation of choice of dyes

In order to understand the environmental performance of the biochars we created, we examined them with anionic and cation dyes commonly used in other studies of environmental adsorbents. The two

Table 1
Model compound chemical properties. All information found from online chemical databases or manufacturer labeling.

| Dye | MW (g/mole) | Empirical formula | pK_a | Absorbance wavelength used (nm) | Maximum water solubility (g/L) | ${\rm Log}~{\rm K_{\rm ow}}$ |
|----------------|-------------|---|-----------|---------------------------------|--------------------------------|------------------------------|
| Crystal violet | 407.99 | C ₂₅ H ₃₀ ClN ₃ | 1.15, 1.8 | 590 | 50 | 1.172 |
| Methyl orange | 327.33 | C ₁₄ H ₁₄ N ₃ NaO ₃ S | 3.47 | 465 | 5 | unknown |

Methyl orange

Fig. 4. Structures of model dyes used to examine biochar adsorption.

dyes we chose, Methyl Orange (MO) and Crystal Violet (CV), are presented in Table 1 and Fig. 4 with some of their basic chemical properties. One important advantage for the use of dyes as model compounds is that they relatively simple to quantify in solution with a UV-visual spectrometer.

The larger chemical structure of each compound is important, but much of the quantitative adsorptive behavior for each one with a surface can be explained by the type, amount, and density of charges in the compound. Both MO and CV have pK_a that should make it such that they remain unprotonated on their most acid active moieties at the pH tested. The biochar, on the other hand, likely will experience surface charge changes from the change of initial pH we used from (6–9).

2.3.2. Adsorption batch experiments

We examined the adsorptive capabilities of each biochar by batch adsorption experiments. Preliminary examinations revealed biochar adsorption equilibrium times of 8 hours and 48 hours for CV and MO, respectively. The dye concentrations tested were 25, 50, 100, 286, and 1000 mg/L for CV and 20, 40, 80, 150, 300 mg/L for MO.

Each experiment was repeated in triplicate and consisted of 14 mL conical vials containing 10 mg of each biochar and 10 mL of each dye concentration at pH values of 6 and 9. These vials were then shaken for the equilibrium time. They were removed from the shaker and centrifuged at 2500 rpm. The supernatant was then sampled and if necessary, diluted, before being analyzed by UV–VIS spectrometer (An et al., 2010; Azami et al., 2012).

2.3.3. Equilibrium adsorption studies

A summary of experiments we conducted to compare environmental performance of biochars is provided in Table 2. Many of the conditions were the same for each dye examined though not all. All four biochar types were examined at these conditions yielding a total of sixteen adsorption experiments (1 $\frac{exp}{pH} \times 2 \frac{pH}{dye} \times 2 \frac{dye}{biochar} \times 4 biochar = 16 exp$). We conducted all experiments at room temperature, which was not precisely

controlled or monitored, but is known from climate control settings to be 24–25 $^{\circ}$ C.

We determined quantitative equilibrium adsorption of biochar with dyes using the batch equilibrium mass balance method to determine the final adsorbed concentration and partition of dye between dissolved and adsorbed phases as shown in Eq. (1). In the equation, $q_e(\frac{\text{mg}}{g})$ is the final equilibrium dye concentration on biochar, $V_{sol}(\text{mL})$ is the volume of dye solution used in an experimental replicate, $c_o(\frac{\text{mg}}{L})$ is the initial dye concentration of the replicate, $c_e(\frac{\text{mg}}{L})$ is the final dye concentration in the water solution after shaking, and $m_{bc}(g)$ is the dry mass of biochar we introduced to the replicate.

$$q_e = \frac{V_{sol}(c_o - c_e)}{m_{bo}} \tag{1}$$

We conducted many preliminary to studies to determine useful ratios between mass of biochar and mass of dye. It was important to determine these ratios in order to ensure that we used a value of c_o , V_{sol} , and m_{bc} which would be able to show a quantitative decrease from the initial concentration (c_o-c_e) while not having c_e be at a concentration which was so low that the UV–Vis spectrophotometer could not distinguish it from background. Reasonable biochar mass to dye mass ratio (BCD = $\frac{m_{bc}}{V_{sol}}c_o = \frac{m_{bc}}{m_{dye}}$) were 20–300 for MO and 10–400 for CV.

3. Results

3.1. Production results and specific surface area

We initially wanted to understand the potential of the TLUD biochar production system, made in developing world type of style, to make biochar with feedstock that are common agricultural waste products. We procured five different biochar feedstock biochar comparison between the TLUD and muffle furnace at 450 °C (MF) methods. Table 3 shows the production results for all five.

We measured all values according to biochar produced from either method and without any further processing (other than cooling) except for BET SSA. For surface area, we did use the same DI wash, crushing, and sieving used for the in depth exploration of PS and CS biochar.

For the TLUD method, we note it was difficult to keep all of the loose material inside of the pyrolysis device. The need to maintain sufficient airflow to sustain the burn meant that screening material at the base of the device could not be too small. As well, even with the use of the chimney secondary incineration of volatiles, lighter organic or ashen material could be entrained and leave out the top. As the purpose of the use of the TLUD was to simulate something close to a low resource setting, we did not make any additional effort to constrain or recapture material leaving by gravity at bottom or entrained in upward exhaust.

The total BET surface areas for all feedstock were higher by the TLUD production method in nearly all cases with the one exception being wheat stover. The MF produced biochar likely did not ever experience pyrolysis at temperatures >450 °C since it was in a controlled condition while the TLUD biochar likely experienced much higher temperatures since the heating came from combustion at the top of the mound of fuel. The higher temperatures resulted in increased mass loss as indicated by production yield while at the same time providing higher BET surface area. The fact that the pecan shell and cotton seeds results in the highest BET surface areas by the TLUD production method led to our selection of them as candidates for further material characterization and adsorption studies.

Table 2Experimental conditions used for generation of batch equilibrium adsorption isotherms.

| Experimental condition | Crystal violet (CV) | Methyl orange (MO) |
|---|---------------------|--------------------|
| initial pH used | 6.0, 9.0 | 6.0, 9.0 |
| biochar to dye mass ratios (m _{bc} :m _{dve}) | 10-400 | 20-300 |
| solvent for dye solutions | DI water | DI water |
| replicate solution volumes (mL) | 10 or 20 | 10 or 20 |
| replicates for each condition | 3 | 3 |
| shaking speed (rpm) | 220 | 220 |
| shaking time (hr) | 8 | 48 |
| solution temperature (°C) | 24–25 | 24–25 |

Table 3

Production summary of five common crop waste biochar produced using either TLUD or MF. All measurements are for biochar shortly after pyrolysis and with any crushing or grinding.

| Feedstock | Bulk bioch | ar density (g/cm³) | Production | yield | Median gra | Median grain size (mm) BET specific surface area (m | | rea (m²/g) | m^2/g) | |
|--------------|------------|--------------------|------------|-------|------------|---|------------------|------------|-----------|--|
| | TLUD | MF | TLUD | MF | TLUD | MF | original biomass | TLUD | MF | |
| Coconut coir | 0.11 | 0.09 | 7.2% | 20% | 1.6 | 1.5 | 0.829 | 210 | 66 | |
| Pecan shells | 0.28 | 0.25 | 11% | 36% | 2.2 | _ | 0.583 | 430 | 43 | |
| Rice husks | 0.13 | 0.13 | 20% | 37% | 1.8 | 1.3 | 0.745 | 140 | 130 | |
| Wheat stover | 0.046 | 0.046 | 8.1% | 18% | 3.8 | 6.7 | 0.360 | 10 | 11 | |
| Cottonseed | 0.21 | 0.18 | 15% | 23% | 3.0 | 2.4 | 22.4 | 560 | 490 | |

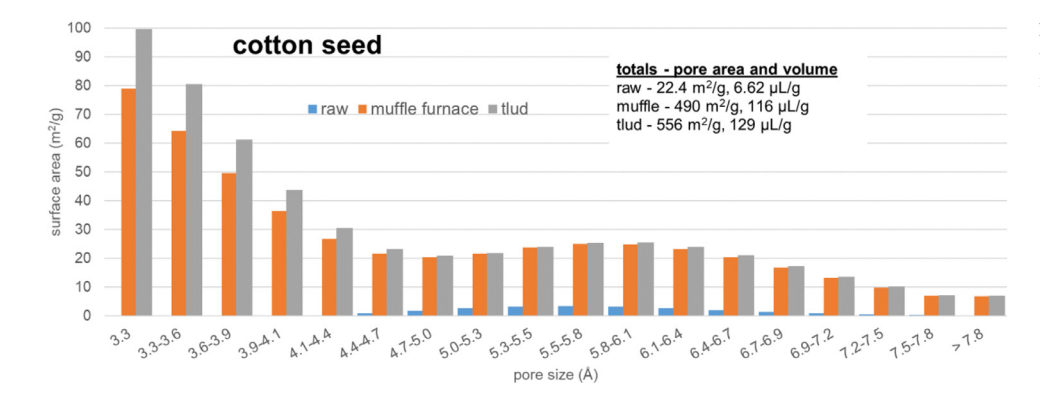


Fig. 5. Surface area and pore volume distribution in raw cottonseed and its biochar according to micropore size.

We examined the original CS material (CS-Raw) and the two biochar for micropore distribution as shown in Fig. 5. CS-Raw has extremely low area and volume of micropores while the CS-TLUD show about half of its total area in pores < 4 Å.

3.1.1. TGA

We summarize comparative TGA-DTG curves for biochar and raw biomass in Fig. 6. By examining the differences between biochar versus the raw material, we can get some sense of what the nature of the pyrolysis is in both types of biochar. The differences in the production of the biochar will provide insight into other material properties of the biochar as well as its environmental performance. We obtained all TGA data for all materials from a Netzsch Jupiter TGA-DSC instrument with sample size 20–30 g in closed crucibles and heating rate 10 °C/min.

To help understand the differences in the curves according to temperatures that the feedstock likely experienced during pyrolysis production of biochar, it helps to have context for biomass components that pyrolyze in particular temperature regions. The work of Yang et al. (2006) is useful in how we chose to understand the components of the original material and when that material was pyrolyzed according to temperature. Yang et al. conducted an examination of biomass by looking at the pyrolysis of pure hemicellulose, cellulose, and lignin on a TGA. Using their analysis, we estimate the pyrolysis of each component to occur in the following ranges—moisture & volatile organics (M & V, < 220 °C), hemicellulose (H, 220–315 °C), cellulose (C, 315–400 °C), lignin (L, 400–895 °C), and char+ash (C+A, whatever remains when T>895 °C). While not absolute, these temperatures provide guide-

lines for biomass component characterization, and we have indicated them in the plots. We quantified the mass losses in each temperature range, based on the TG plots, in Table 4.

3.1.1.1. Cottonseed. Considering the TGA instrument itself as a highly controlled form of pyrolysis, it is simulating something similar to what is happening to MF450 and TLUD biochar. Looking at the raw biomass in this idealized pyrolysis, we see that CS has large mass losses distributed about equally between the three biomass component regions with H, L, and C all contributing about 20–23%. A look at the DTG lines for CS show what looks to be a shouldered maximum in the H region at $\sim\!270\,^{\circ}\text{C}$ and a definitive maximum in the C region at 335 °C. The presence of the shoulder suggest that C in cottonseed may be starting to pyrolyze before 315 °C. The DTG falls off very quickly at all temperature > 335 °C. Small maxima may exist in the L region, but they are hard to discern. The mass losses in the raw CS biomass are substantial for all three biomass components, and the losses occur in localized temperature regions for H and C. The L component region falls off very gradually and over a wide range of temperature.

Moving to the CS biochar, we see that not even 10% of its mass is lost until 370 °C in the MF450 and not until 400 °C for CS-TLUD. In contrast to the biochar, nearly half of the overall mass is pyrolyzed in the H+C region in the raw biomass. The small mass loss at $<400\,$ °C indicates that both pyrolysis processes, MF450 and TLUD, pyrolyzed nearly all of the H and C in the original material. When comparing the two biochar together, the MF450 shows a local DTG maximum in the L region at 525 °C that is not present in the TLUD biochar. Thus, it likely that the CS-

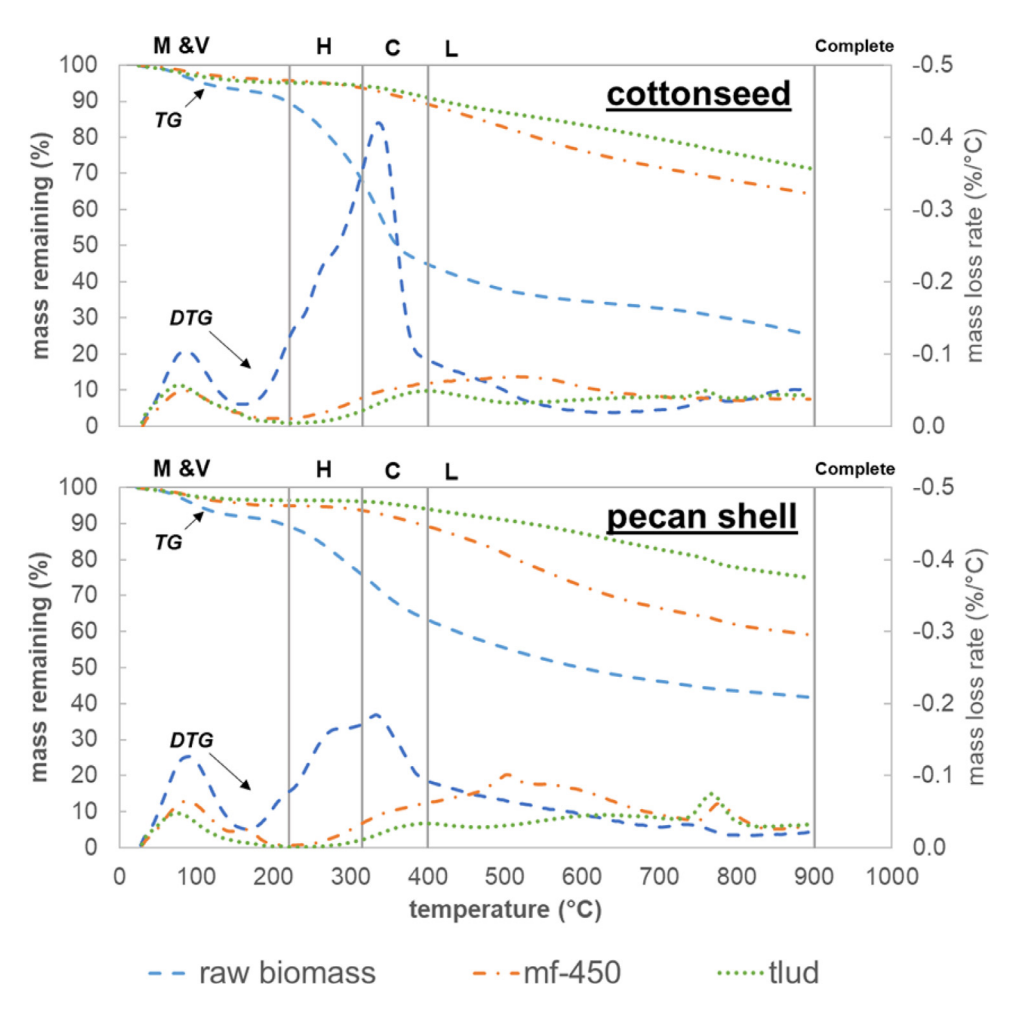


Fig. 6. Combined TGA-DTG plots for original biomass, biochar generated by muffle furnace at 450 C (MF-450), and top-lit updraft (TLUD). Loss region divisions used are 220 °C (division between hemicellulose loss region and moisture-volatiles, M & V), 315 °C (division between hemicellulose loss region and cellulose region, H, C), and 400 °C (division between cellulose loss region and lignin region, L). We note that other authors take 895–900 °C and higher as the region, where any further losses would come only from ash content. Thus at this temperature, pyrolysis is essentially complete. Upper lines are thermogravimetric (TG) mass loss lines while lower lines are derivative TG (DTG) lines.

Table 4Mass loss fraction within temperature ranges on TGA plots.

| Source of mass loss | Moisture & volatile organics (M & V) | Hemicellulose pyrolysis (H) | Cellulose pyrolysis (C) | Lignin pyrolysis (L) | Remaining mass |
|-------------------------------|--------------------------------------|-----------------------------|-------------------------|----------------------|----------------|
| temp range (°C) cottonseed | < 220 | 220–315 | 315-400 | 400-895 | > 895 |
| raw | 10% | 22% | 23% | 20% | 25% |
| mf450 | 4.3% | 2.1% | 4.5% | 25% | 64% |
| tlud | 4.7% | 0.9% | 3.3% | 20% | 71% |
| pecan shell | | | | | |
| raw | 11% | 14% | 12% | 21% | 42% |
| mf450 | 5.1% | 1.3% | 4.4% | 30% | 59% |
| tlud | 3.4% | 0.30% | 2.2% | 19% | 75% |

TLUD biochar reached temperatures much higher than 450 $^{\circ}$ C in many parts of the pyrolyzing mass within the device. The higher sustained temperature in the TLUD is further indicated by the slightly lower L region mass loss compare to MF450 and the fact that the remaining mass at TG pyrolysis completion (~900 $^{\circ}$ C) is noticeably higher in CS-TLUD (71%) compared to CS-MF450 (64%). For both CS-MF450 and – TLUD, more material, primarily lignin, was not fully pyrolyzed by either method. Differences in other properties and environmental performance of CS biochars may depend on small differences in lignin pyrolysis extent between MF450 and TLUD.

3.1.1.2. Pecan shell. The raw PS biomass is distinct from the raw CS in that it will either have higher L content in absolute sense, higher L relative to H+C, or both. The mass lost in the H+C region is only 26% for PS compared to 50% for the CS. Despite the lower H+C content, the same shouldering on the DTG plot between the H and C regions is also

seen in PS that was seen in CS. The difference in the residual mass (> 900 $^{\circ}$ C) for the PS versus CS is also telling. Raw CS, when pyrolyzed to 900 $^{\circ}$ C has only 25% mass remaining compared to 42% in PS.

There are at least two possible reasons for the higher residual mass in PS. One is the increased quantity of lignin in the raw material PS compared to CS. All of these biomasses, when pyrolyzed, lose material in the form of CHON compounds, and the result is a higher degree of carbonization and aromatization in the final biochar. Lignin, of the three components, preserves the most amount of its original material because it is more aromatic by nature (Yang et al., 2006). Thus, the increased amount of lignin in the original biomass leads to higher residual mass and potentially higher overall production yield of biochar. Table 3 indicated the production yield of PS-MF450 was higher than CS-MF450, but the yields were much closer for the TLUD.

Second is the possibility that PS has higher native ash/mineral content compared to CS. Higher ash content means more material that can-

not be pyrolyzed, and that material would thus remain at the end of the TGA. Zhang et al. (2016) reported a PS crop waste ash content of 1.5% while Huang et al. (2017) reported CS meal had ash content of 7.1%. We did not directly measure the bulk ash content in these materials, but based on these literature values, we surmise the reason for the higher residual material at TGA T > 900 °C is better explained by higher L content rather than higher ash content.

Looking towards the PS biochar, the difference in the TG curves, especially at T > 400 °C, is greater between the two biochar types and the raw biomass for PS compared to CS. PS-MF450 has a local DTG maximum at 505 °C, not far away from the maximum in CS-MF450 at 525 °C. Both PS-MF450 and PS-TLUD have a second L region maximum around 760-780 °C. The TLUD biochar DTG maximum is at a slightly lower temperature (left shift). These trends, in combination with the higher L region mass loss for MF450 (30%) compared to TLUD (19%), point to a similar explanation between the two biochar production methods. The maximum temperature reached in the TLUD is certainly higher than the lab-limited 450 °C in the MF. In the raw PS, there is only a small amount of pyrolysis mass loss in the L region before 450 °C (only 4% of the total 21% occurred). Thus, the MF450 leaves a fair amount of L either unpyrolyzed or not fully pyrolyzed through the temperature limitation. However, the PS-TLUD biochar is not fully carbonized as evidenced by the additional mass loss that occurs in its TGA plot. The majority of its L region mass loss occurs at > 600 °C (loss of 14% 600-895 °C), which suggest that the highest temperature much of the material reaches inside of the TLUD is in the range of 600-650 °C.

3.1.2. SEM/EDS

Physically biochar consists of a network of pores on a carbon based body (Herbert et al., 2012). The porous nature of the biochars is a major factor in its adsorption capability and is strongly influenced by biomass precursor and pyrolysis methods (Yang et al., 2015a). Each pore contributes to the biochar's overall surface area and as such it creates additional reactive molecular sites capable of adsorption.

All SEM images of biomass original material and final biochar are presented in Fig. 7. The PS-Raw biomass consists of granules covered in indents along with a small amount of fibrous materials, while the CS-Raw biomass also consisted of indented granules with a multitude of fibers (Fig. 7a and b). Cottonseed is one biomass stream coming out of local cotton gins in the Texas Panhandle. Residual fibers from the ginning process are clearly still present when the material we examined the biomass closely by the naked eye, and those fibers show up strongly on the SEM as well. The ginning process seeks the lint as the primary agricultural product with cottonseed being a byproduct or sometimes considered a waste product.

Fig. 7c and e shows that both the TLUD and MF450 pecan shell biochars contain a vast amount of differently sized pores on their surfaces. These pores were either not present or not visible in the original biomass. We performed surface pore size analysis on the image. The analysis revealed that the PS-TLUD biochar had pore sizes ranging between 1.003 and 15 μm with the majority falling in the 5–10 μm range. The PS-MF450 biochar has a broader array of pore sizes ranging between 3.307 and 30 μm with the majority of falling within the 5–15 μm range.

Fig. 7d and f shows the surfaces of both the CS-TLUD and CS-MF450. These materials contain a semi-uniform array of pores across their surfaces. The CS-TLUD pores fall into a range from 1.990 to 20 μm while the CS-MF450 particles are in the 3.094–25 μm range. Pore size analysis reveals that both biochars have most of their pores falling within the 5–10 μm range. Visually the two CS biochars look nearly the same.

The larger range of pore sizes occurring in the PS and CS MF biochars can be attributed to lower pyrolysis temperatures used in the muffle furnace. We surmise that generally higher pyrolysis temperatures occur in the TLUD device. The pore size analysis show that the TLUD biochars have a majority of their pores falling in the 5–10 μ m range, and this allows the pores to litter the surface of the biochar while occupying less

Table 5Biochar and raw material EDS analysis taken from previous SEM images.

| Component | Pecan sh | iell | | Cottonse | Cottonseed | | | |
|---------------|----------|-------|-------|----------|------------|-------|--|--|
| | Raw | TLUD | MF450 | Raw | TLUD | MF450 | | |
| Elements (%) | | | | | | | | |
| C | 56.23 | 74.42 | 73.32 | 53.02 | 82.03 | 74.72 | | |
| 0 | 42.62 | 20.23 | 26.14 | 45.8 | 12.24 | 21.92 | | |
| Mg | 0.4 | 2.69 | X | X | 1.86 | 0.91 | | |
| Si | X | X | X | 0.2 | X | X | | |
| S | X | X | X | 0.1 | X | X | | |
| P | 0.11 | 0.31 | X | 0.18 | X | X | | |
| K | 0.44 | 1.07 | 0.23 | 0.55 | 3.84 | 2.45 | | |
| Ca | 0.19 | 1.28 | 0.31 | 0.16 | X | X | | |
| Groups and ra | atios | | | | | | | |
| C:0 | 1.32 | 3.68 | 2.80 | 1.16 | 6.70 | 3.41 | | |
| C+O (%) | 98.9 | 94.7 | 99.5 | 98.8 | 94.3 | 96.6 | | |
| ash (%) | 1.15 | 5.35 | 0.540 | 1.18 | 5.73 | 3.36 | | |

X=component not found in EDS scan.

space than larger pores. The CS biochars have a moderately uniform array of 5–10 μm pores across its surface while the PS biochars have a more diverse array of pore sizes across its surface. The uniform nature of the pores on the CS biochar directly contribute to an increased overall surface area. These trends support the BET data which shows that the TLUD biochars have a larger surface area than the MF, and CS biochar has a greater surface area than PS.

The EDS analysis of the four biochars and original provided in Fig. 7 images yields an elemental composition of primarily carbon with trace amounts of Mg, P, K, and Ca as shown in Table 5.

Carbon to oxygen (C:O) ratios for PS are 3.7 and 2.8 for TLUD and MF450, respectively. The same comparison in CS is 6.7 (TLUD) and 3.4 (MF450). Both of these ratios indicate a higher degree of carbonization for the TLUD process as compared to the muffle furnace at 450 °C process. Carbon content increase at the expense of oxygen-containing functional groups in the original material (examples like alcohols, carboxylic acids, and ketones). The difference between the two processes is greatest in CS as compared to PS. The surface elemental analysis suggests that there should be fewer surface functional groups overall in the TLUD biochar compared to the muffle furnace biochar.

The analysis here shows that overall surface mineral content (Mg, P, K, Ca) is higher in TLUD biochar (CS 5.7%, PS 5.4%) relative to MF450 (CS 3.4%, PS 0.54%). We suspect that the ultimate reason for this is that more carbonaceous components were lost in the TLUD to concentrate the ash that remained. We note that EDS does not provide hydrogen (H) content, and inclusion of this element could alter the analysis.

3.1.3. FTIR

To investigate the effects of pyrolysis, we analyzed the FTIR spectra of raw pecan (Fig. 8) and cottonseed (Fig. 9), and their biochars from TLUD and MF450. Both raw sample demonstrated very similar functional groups, which notably exist in a carbohydrate polymer.

We observed O-H stretching (at $\sim 3300~\text{cm}^{-1}$), C-H2 stretching (at 2900 cm⁻¹), C-C vibration in aromatic ring (1600 cm⁻¹), C-C and C-O skeletal vibration (at 1290 cm⁻¹) and C-O-C stretching (at 1290 cm⁻¹) associated with the cellulose of raw PS and CS. FTIR spectra also demonstrate that pyrolysis removed most of the functional groups and left the carbon backbone in the cellulose. EDS analysis of the samples supports the decrease in functional groups.

PS biochar produced in the muffle furnace contains some of the left over functional groups which are mostly eliminated in pyrolysis. As shown in Fig. 9, weak signals of the C-H2 stretching (at 2900 cm⁻¹), C-C vibration in aromatic ring (1600 cm⁻¹) and C-O-C stretching (at 1290 cm⁻¹) were observed in the Pecan shell biochar from muffle furnace. By comparison, in the PS-TLUD all the functional group almost disappear except the peak of the C-C vibration in the aromatic ring (1600 cm⁻¹). FTIR data indicate both PS biochar contain predominantly

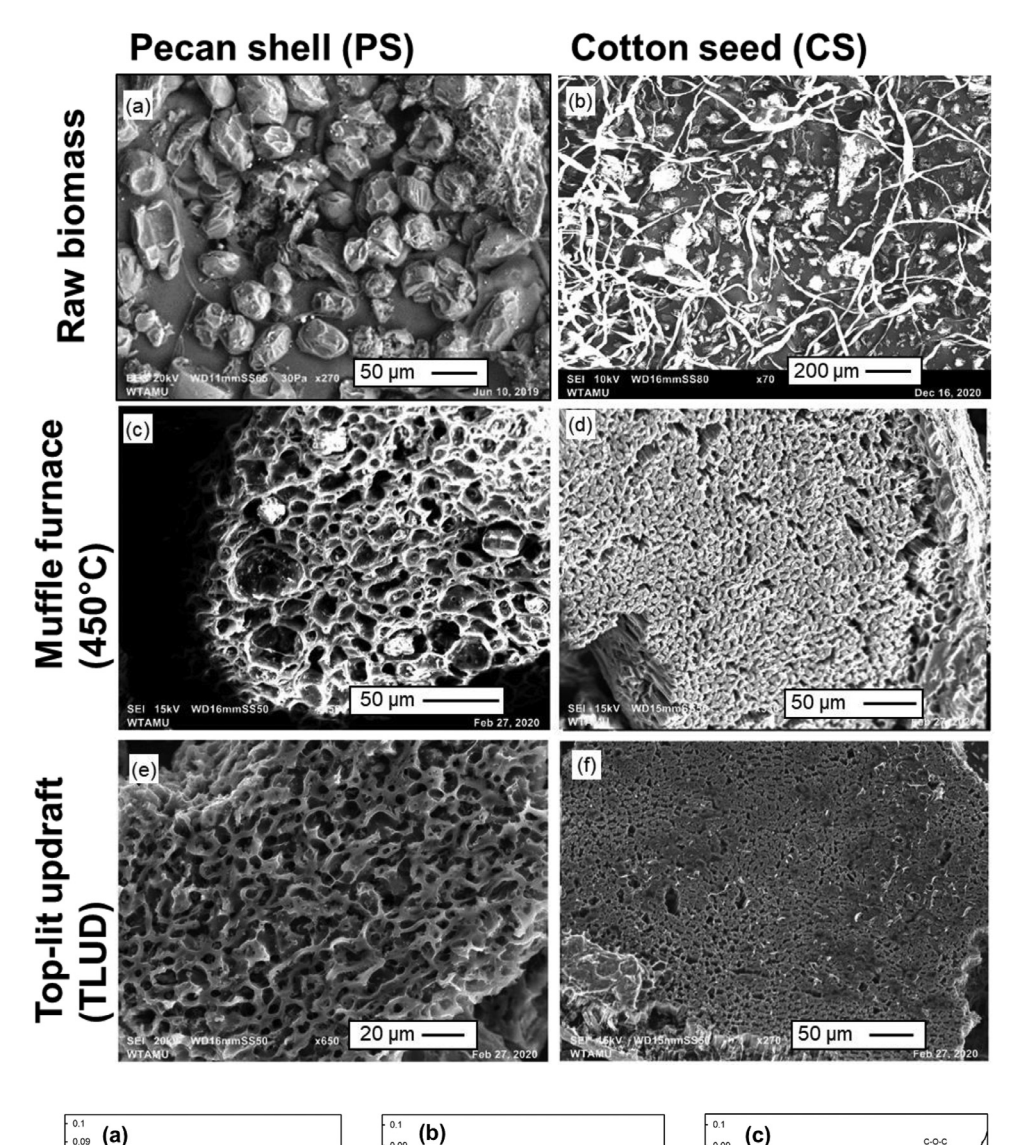


Fig. 7. SEM images of raw biomass materials used to make biochar.

Fig. 8. FTIR spectra of (a) Raw PS (b) PS-MF450 (c) PS-TLUD. Peaks observed at 2300 $\rm cm^{-1}$ correspond to $\rm CO_2$ in air.

carbon in the structure (at 1600 cm⁻¹). Comparing the FTIR data of the both PS-MF450 and-TLUD, it shows biochar from TLUD loses more of its functional groups which is also supported by its high ash content (Table 5) and low surface area (Table 3).

Wavenumber (cm⁻¹)

0.08

0.07

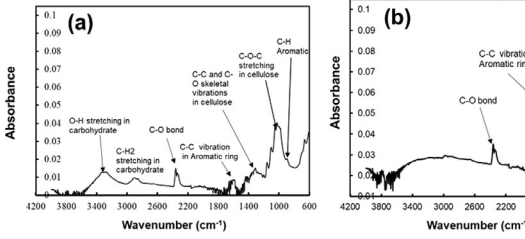
Cottonseed biochar from both MF450 and TLUD contain primarily a C-C vibration as aromatic rings ($1600~\rm cm^{-1}$). Both CS biochars show a weak signal of C-O-C stretching (at $1290~\rm cm^{-1}$), which is much diminished compared to the raw CS. FTIR data indicate both MF450 and TLUD biochar show similar structure which is also supported by the similar surface ash content (3.4–5.7%, Table 5) and surface area data ($560~\rm m^2/g$ and $460~\rm m^2/g$ in Table 3). We note that Brewer et al. (2017) determined what occurs when biomass pyrolysis occurs in the presence of a minor oxygen environment ($5\%~\rm O_2$ in $\rm N_2$) such as what is likely in the TLUD. They determined that this small bit of oxygen did not increase either overall biochar oxygen content or oxygen-containing functional groups, and that finding seems to hold in our dataset. The TLUD, being a merely

low oxygen environment, did not show any oxygen increases relative to MF450.

Biomass is comprised primarily of three lignocellulistic components: cellulose, lignin, and hemicellulose (Yang et al., 2015a). Like other complex organic molecules, lignin and hemicellulose are amorphous (Johar et al., 2012b). Cellulose, however, contains crystalline matrices of linear D-glucose chains that can be detected and assessed by x-ray diffractometry (Herbert et al., 2012; Yang et al., 2015a). During pyrolysis depolymerization of cellulose occurs in the raw materials affecting final quantities in the biochar (Rojith and Singh, 2013). The assessment of the cellulose crystallinity index (CrI) and crystallite size (t) in the biochars are of value as they may have an impact on absorption performance.

In nature cellulose I is the most commonly encountered of the cellulose crystalline allomorphs. It is comprised of two distinct crystalline forms: $I\alpha$ and $I\beta$. $I\alpha$ is the dominant component in bacterial and algal

Wavenumber (cm⁻¹)



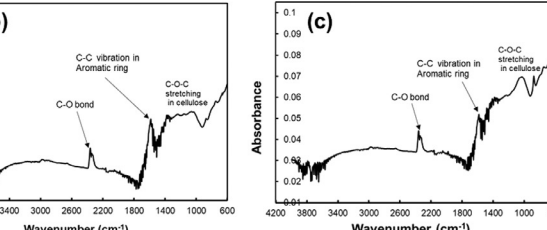


Fig. 9. FTIR spectra of (a) Raw CS (b) CS-MF450 (c) CS-TLUD. Peaks observed at 2300 $\rm cm^{-1}$ correspond to CO $_2$ in air. XRD.

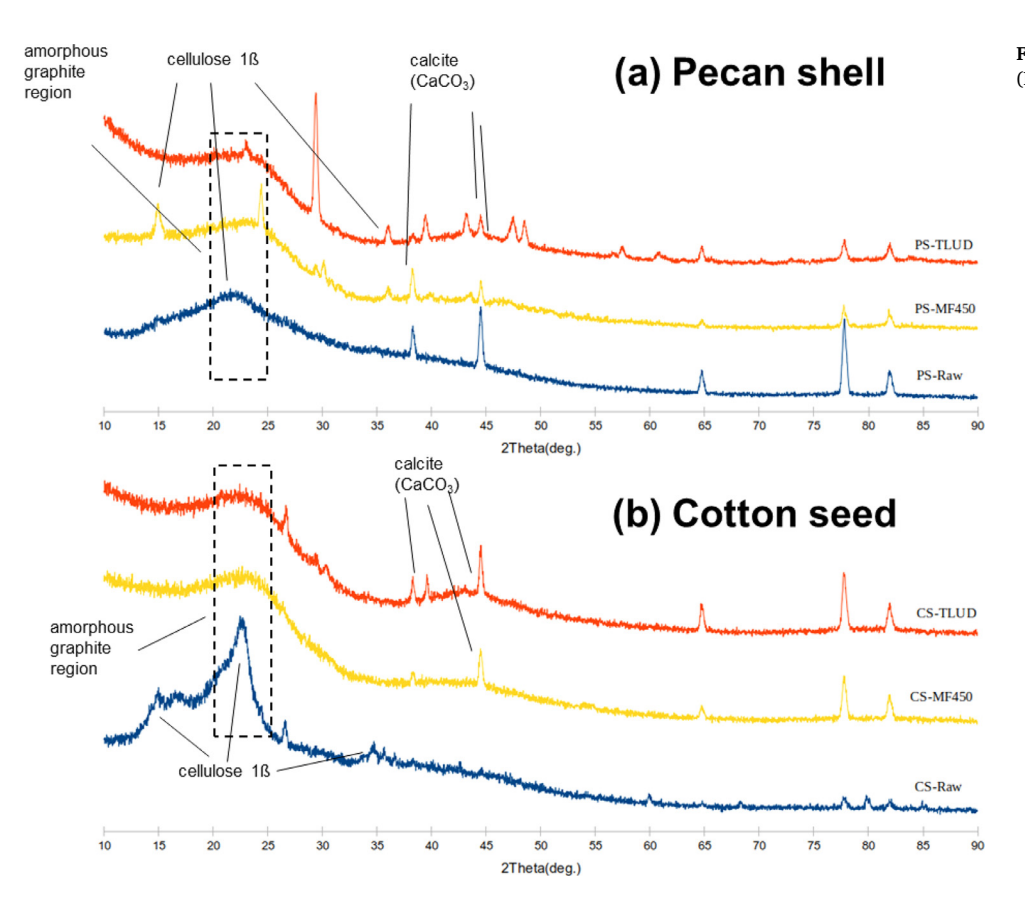


Fig. 10. XRD diffractogram for (a) pecan shall (PS) and (b) cotton seed (CS).

celluloses while I β dominates celluloses in higher plants due to it being the major component in the secondary wall of plant cells (Atalla and VanderHart, 1984; Nam et al., 2016). As PS and CS both come from higher plants, we assessed the dominating cellulose I β by XRD.

The XRD patterns for the raw PS and CS as well as their respective TLUD, and MF biochars are shown in Fig. 10.

Each pattern reveals the crystalline peaks of cellulose I θ around $2\theta=16^\circ$, 22° , and 35° and calcite crystalline peaks at $2\theta=39^\circ,43^\circ$, and 44° (Herbert et al., 2012; Johar et al., 2012a; Liu et al., 2017; Yang et al., 2015a). The curve from $2\theta=20^\circ$ to 25° is representative of amorphous graphite and becomes more prominent after pyrolysis implying a reduction in crystallinity(Han et al., 2015).

The crystallinity index and crystallite sizes were calculated using the Segal (Eq. (2)) and Scherrer (Eq. (3)) equations respectively (G and Singh, 2013; Jasiukaityte-Grojzdek et al., 2012; Nam et al., 2016).

$$CrI = \frac{I_{200} - I_{am}}{I_{200}} \times 100 \tag{2}$$

The Segal equation calculates crystallinity indices (Crl) using the intensity of the amorphous background scatter (I_{am}) at $2\theta=18^\circ$ and the maximum intensity of the 200 plane associated with cellulose $I\beta$ (I_{200}) at $2\theta=22.7^\circ$ in arbitrary units.

$$\tau = \frac{K\lambda}{\beta\cos\theta} \tag{3}$$

Table 6Material XRD assessment.

| Material | I ₀₀₂ | FWHM (rad) | I _{am} | CrI (%) | τ (Å) |
|----------|------------------|------------|-----------------|---------|--------|
| PS-Raw | 4391 | 0.039 | 2889 | 34.206 | 38.272 |
| PS-TLUD | 1907 | 0.052 | 1746 | 8.443 | 28.897 |
| PS-MF450 | 4008 | 0.423 | 3513 | 12.350 | 3.551 |
| CS-Raw | 5200 | 0.025 | 4054 | 22.038 | 60.686 |
| CS-TLUD | 1752 | 0.163 | 1649 | 5.879 | 9.240 |
| CS-MF450 | 3824 | 0.369 | 3598 | 5.910 | 4.073 |

The Scherrer equation calculates crystallite size (τ) perpendicular to a lattice plane. Where β is the full width at half maximum (FWHM) of the diffraction peak in radians, θ is the peak diffraction angle, λ is the X-ray radiation wavelength, and K is the correction factor set at 0.9 (Langford and Wilson, 1978). The 200 plane at $2\theta=22.7^{\circ}$ refers to the width of a cellulose crystallite and was used to calculate the raw and biochar crystallite sizes (Jasiukaityte-Grojzdek et al., 2012; Nam et al., 2016).

As seen in Table 6, after pyrolysis both the crystallinity index and crystallite size decrease. This is most likely the result of cellulose depolymerization reducing the final amount in the biochars. The MF biochar varieties have a slightly higher crystallinity than that of the TLUD

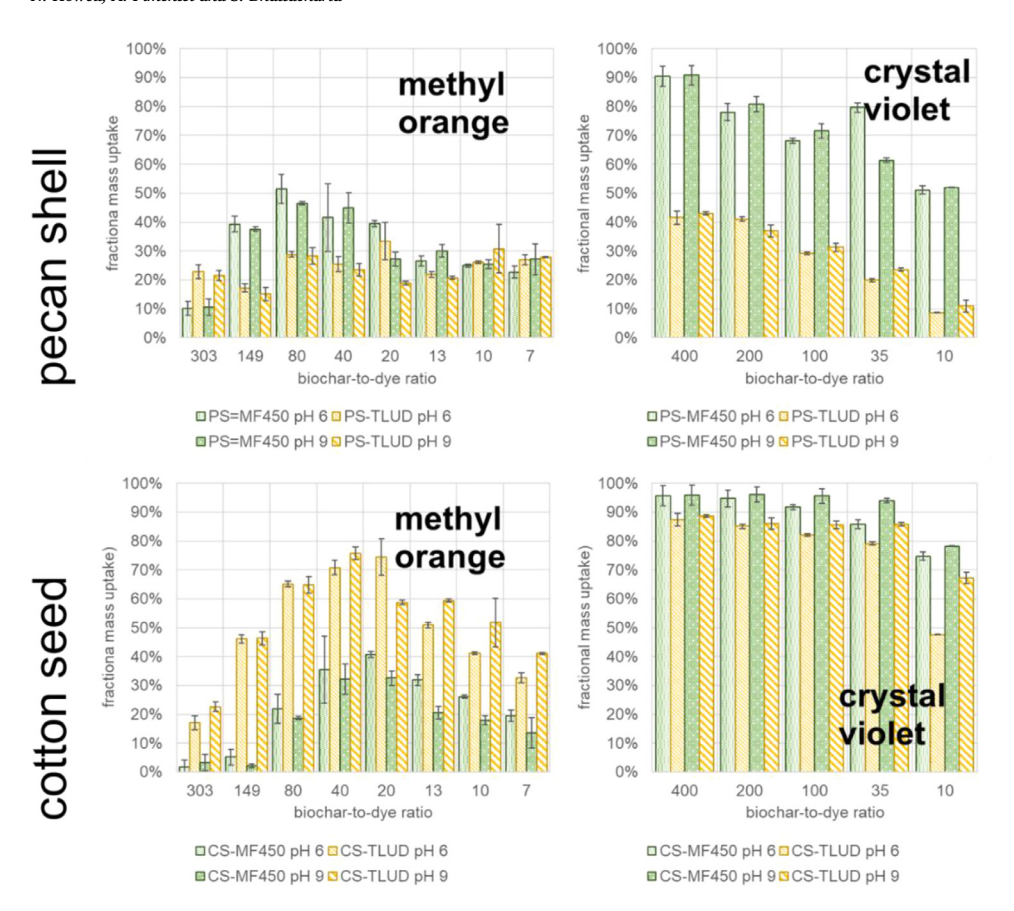


Fig. 11. Mass fraction of dye taken up by biochar adsorbent. Biochar-to-dye ratios indicate the total amount of biochar in a vial divided by the total mass of dye ($V_{\rm vial}C_{\rm o}$). Error bars indicate the standard deviation amongst the three replicates used for condition.

biochars. This can be attributed to a lower amount of cellulose undergoing depolymerization due to the lower pyrolysis temperature used in the muffle furnace. As seen in the chart in the TGA plots, the initial amount of cellullose is reduced after pyrolysis in greater measure in TLUD vs MF450. The thought that more cellulose is pyrolyzed via the TLUD method is thus supported by the XRD assessment showing a decreased crystallinity and crystalite size in the materials.

3.2. Adsorption performance and isotherms

3.2.1. Exploration of dye adsorption in this study

The direct information on the adsorptive potential of the biochar materials with the test dyes comes from the replicate experiments where biochar mass was held constant and initial dye concentration ($c_{\rm e}$) was varied. The measured parameter was the remaining concentration ($c_{\rm e}$, mg/L) in each vial for the 16 experimental combinations. We examined the adsorption from the experiments first by comparing the experiments against each other by the uptake fraction of dye in each experimental condition (Fig. 11). We then modeled the adsorption isotherms from all experiments ($q_{\rm e}$, mg/g vs. $c_{\rm e}$ mg/L) using several models seen in the literature for biochar, dyes in water, or both. We present the best model parameters and fit data in Table 7 and the isotherm data in the context of the best-fit model for each biochar, pH₀, dye combination in Fig. 12.

3.2.2. Mass uptake fraction of dyes

Fig. 11 provides a detailed look at the fractional uptake of dye onto each biochar mass according to experimental setup. We define the fraction mass uptake (f_{up}) and the biochar-to-dye ratio (BCD) in Eqs. (4) and (5). Variables in the equations are as follows: mass of biochar is m_{bc} , initial concentration is c_o , final equilibrium adsorbed dye concentration is q_e , total mass of dye in the adsorption vial is m_{dye} , so-

lution volume used in experiment is V.

$$f_{up} = \frac{q_e m_{bc}}{c_o V} \tag{4}$$

$$BCD = \frac{m_{bc}}{m_{dve}} = \frac{m_{bc}}{c_o V} \tag{5}$$

The x-axis in the plots is the BCD ratio, which decreases from left to right indicating that c_o used in each case is increasing (BCDand c_o inversely related). There is more starting mass of dye in each vial moving towards the right. We examine the effects of pH $_o$, production method, dye adsorbate, and BCD on f $_{\rm up}$ for each biomass.

The yellow bars are for $p\dot{H}_0$ 6 and 9 in the TLUD while the green indicate the same for MF450 biochar. The left-most bar in each grouping is the lower pH_0 6. A more detailed explanation of trends in the plots is found in the supporting information (SI).

We find three summary effects from the analysis. First, is the effect of initial solution pHo. We would expect that there would be some noticeable change in mass uptake via adsorption due to the charged nature of the two dyes, one being anionic and one cationic. To the degree that negative surface functional groups provide the adsorption mechanism for cationic crystal violet, there should be a pHo effect. A higher pHo should be favorable for CV adsorption because there are less H+ ions to compete with its adsorption. However, there is not much effect of pH₀ for any of the biochar types for CV. In some instances, the higher initial pH made a slight difference, but by-and-large it is not substantial. The larger pH_o effect was found in MO, which generally should not be greatly impacted by the availability of negative surface functional groups. In most instances, the lower pH₀ had the higher mass uptake. We explain the effect by the greater prevalence of H+ ions that could neutralize negative surface functional groups and thereby diminish electrostatic repulsion for anionic MO.

Second, is the effect of the biochar production method. The trend seen in the data is that the production method we used has a noticeable

Table 7 Adsorption model fit data for all conditions studied. K_p (L/kg) indicates the mean equilibrium partition coefficient (q_e/c_e) seen across all points in the isotherm. R^2 indicates the goodness of fit for log-log plots of q_e vs. c_e data. K_f and n are Freundlich capacity factor and affinity factors, respectively.

| experimental conditions | | best mod | el fit data | | model fit | model fit statistics | | | | |
|-------------------------|----------------|-----------------|-------------|------------------------------------|-----------------------|----------------------|-------------|--------------|-------|--|
| Adsorbate | adsorbent dye | pH _o | model | model parameters | parameter values | R^2 | RMSE (mg/g) | RRMSE (mg/g) | ARE | |
| CS-TLUD | crystal violet | 6 | LMR | q _m , K _L | 55.9, 0.0212, - | 0.999 | 0.52 | 0.45 | 5.6% | |
| | | 9 | KRM | k_1 , k_2 , q_m | 0.127, 18.9, 61.1 | 1.000 | 0.92 | 1.46 | 0.38% | |
| | methyl orange | 6 | SPS | n, K _s , q _m | 0.312, 9.05E-07, 42.5 | 0.981 | 2.44 | 3.09 | 30% | |
| | | 9 | TMK | B, K _T ,- | 17.7, 0.0398, - | 0.981 | 3.09 | 3.57 | 46% | |
| CS-MF450 | crystal violet | 6 | FRN | n, K _F ,- | 1.75, 2.87, - | 1.000 | 0.45 | 0.34 | 7.6% | |
| | | 9 | LMR | q _m , K _I | 88.6, 0.0257, - | 1.000 | 0.40 | 0.27 | 4.8% | |
| | methyl orange | 6 | SPS | n, K _s , q _m | 0.38, 7.55E-07, 28.1 | 0.994 | 0.92 | 1.16 | 38% | |
| | | 9 | DBK | q _m , B | 18.8, 3.81E-03, - | 0.981 | 1.09 | 1.26 | 24% | |
| PS-TLUD | crystal violet | 6 | FRN | n, K _F | 2.92, 2.25, - | 0.986 | 0.66 | 0.74 | 14% | |
| | | 9 | SPS | n, K _S , q _m | 1.69, 0.0525, 30.6 | 0.991 | 0.65 | 1.03 | 7.7% | |
| | methyl orange | 6 | FRN | n, K _F | 0.937, 0.0226, - | 0.980 | 1.85 | 2.14 | 16% | |
| | | 9 | KRM | k_1 , k_2 , q_m | 0.00436, 27.7, 52.4 | 0.993 | 1.16 | 1.46 | 49% | |
| PS-MF450 | crystal violet | 6 | KRM | k_1, k_2, q_m | 0.0556, 32.4, 51.2 | 0.999 | 0.75 | 1.19 | 11% | |
| | | 9 | FRN | n, K _F | 1.41, 0.652, - | 0.999 | 0.69 | 0.80 | 15% | |
| | methyl orange | 6 | SPS | n, K _s , q _m | 1.20, 0.00230, 73.2 | 0.961 | 2.21 | 2.80 | 105% | |
| | | 9 | LMR | q_m , K_L ,- | 157, 3.03E-04, - | 0.958 | 2.27 | 2.62 | 82% | |

Model names: SPS=Sips, FRN=Freundlich; LMR=Langmuir, TMK=Temkin, DRK=Dubinin-Radushkevich, KRM=Krishnamuriti. Model parameters with units: q_m (mg/g), k_1 (L/mg), k_2 (unitless), B=RT/b_T (mg/g),K_F [(mg/g)/(mg/L)^{1/n}], K_s [(mg/g)/(mg/L)^{1/n}], K_L (L/mg), K_T (L/mg). Model fit statistics: R2=goodness of fit, RMSE=Root mean square error, RRMSE = Relative RMSE, ARE = Absolute relative error. For all Temkin and Dubinin-Radushkevich models, temperature was taken to be T=25 °C (298 K).

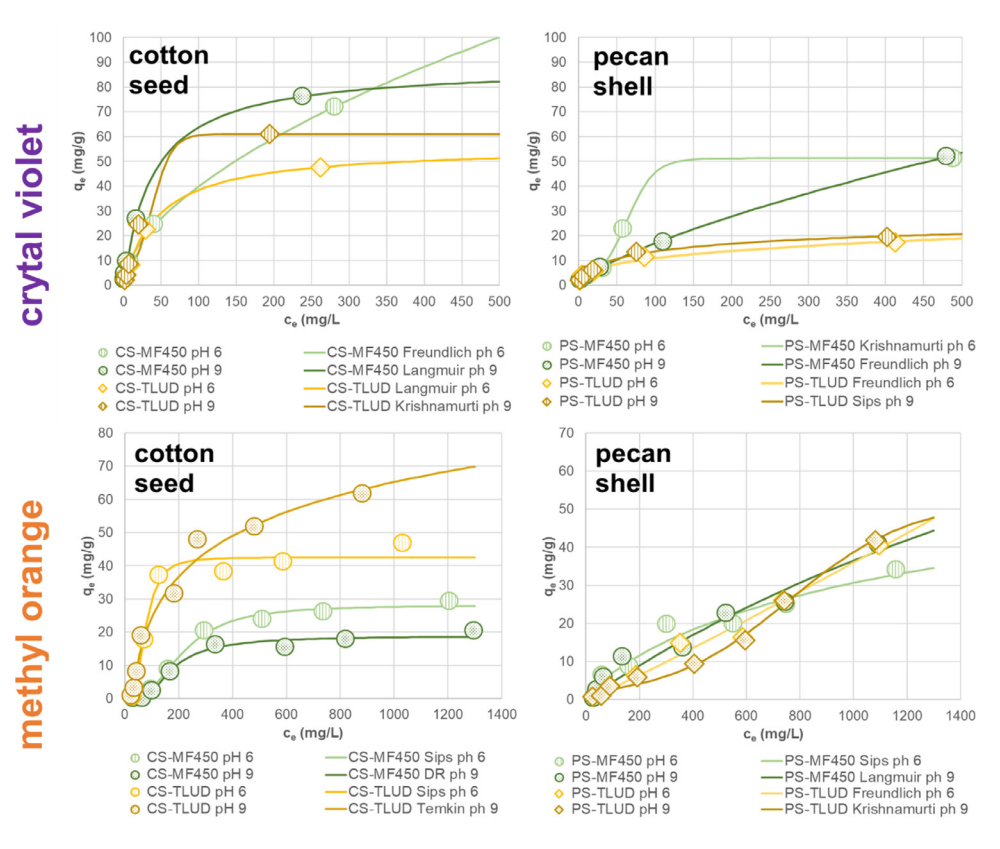


Fig. 12. Adsorption isotherm data with best-fit models for crystal violet (top two panels) and methyl orange (bottom two panels). All points are measured data with biochar type and initial pH (pH_o) as shown. All lines are isotherm models corresponding to a fit of the data that matches the same biochar type and pH_o . The name of the best-fit isotherm type is shown as well. Other models fit reasonably well to the isotherm data besides these, and the selection of the model in each is made entirely on fit statistics indicated elsewhere.

effect for both feedstock as evidenced by the two dyes. But the effect is different for the two biomasses. For the pecan shell, the MF450 biochar is hugely better for adsorption of CV compared to TLUD biochar, about twice as good on average. For the MO, the MF450 is sometimes better and other times has about the same adsorption ability as the TLUD. In the cottonseed, the TLUD biochar is 2–3 times better in MO, and the MF450 in CS is only slightly better on CV. The effect can be summarized in saying that for PS, the MF450 production method increases the adsorptivity but mostly for CV while in CS, the adsorptivity is increased primarily on the TLUD biochar but mostly for MO. Different production

methods create more strongly adsorbing biochar for cottonseed versus pecan shell. Something inherent to each kind of biomass is causing the different behaviors in biochar products.

The third trend concerns the differences in dyes on the four biochars. CV adsorbs more favorably in general to all biochars, and the adsorptive strength is generally high irrespective of the biochar to dye mass ratio (BCD). MO is generally weaker with adsorptive mass uptake never exceeding 50% for any biochar except for CS-TLUD. Also in contrast to CV, the MO has maximum mass adsorption fraction at the middle range of BDR that we tested (13–80). There is not the consistent to slightly chang-

ing mass uptake seen with CV dye. The dose of dye relative to biochar matters for MO uptake but not very much for CV uptake. These differences suggest different adsorption mechanisms or different enthalpies of adsorption (ΔH_{ads}) for the different dyes. We propose that the different chemical contexts of the adsorbate (either CV or MO) drive differing surface interactions that may indicate that separate regions of the surface are accessed by each dye.

3.2.3. Adsorption isotherm modeling

We searched for common adsorption to isotherms to describe out data q_e vs. c_e data. The use of model choice and model fitting to find the best fitting model should provide additional insight into adsorption mechanisms. We will explain this process by first examining the adsorption models that we used for the data. We note that the most common isotherms used for water treatment are Langmuir and Freundlich models. Early on in the analysis, we discovered that many of our isotherm datasets were not concave down in shape, which is what is generally required for use of Langmuir and Freundlich models. The concave down nature is indicative of a Brunauer's Type I isotherm, but many of ours seemed closer to a Type II or V isotherm, one of the S-shaped isotherms which have become more noticeable in recent studies on environmental adsorbents (Ayawei et al., 2017; Chu, 2021; Inglezakis et al., 2018).

3.2.3.3. Isotherms models. Langmuir. The Langmuir model is provided as Eq. (6). It is based on fundamental mechanisms, presumes a monolayer coverage of adsorbate molecules, and is a two-parameter model with $q_e\ (mg/g)$ as the predicted adsorbed concentration, $c_e\ (mg/L)$ as the equilibrium solution concentration, $K_L\ (L/mg)$ as the Langmuir coefficient, and $q_m\ (mg/g)$ as the maximum adsorbate concentration.

$$q_e = q_m \frac{K_L c_e}{1 + K_L c_e} \tag{6}$$

Freundlich. The Freundlich model is provided in Eq. (7). It is two-parameter empirical model whose value lies in its ability to describe experimental data well and consistently when they make a concave down (Type I) isotherm. It has two model constants, K_F [(mg/g)/(mg/L)^{1/n}], the Freundlich constant, and the affinity parameter n (dimensionless). The constants are often interpreted where K_F indicates the general capacity of the adsorption while n indicates the level of affinity adsorbate and adsorbent have for each other. A smaller value of n raises the value of the 1/n exponent. The higher 1/n value leads to higher partitioning of the adsorbate to the adsorbent at a given concentration (Dada et al., 2012). Thus, the smaller the value of n, the higher the affinity or cooperation between adsorbent and adsorbate. Inglezakis et al. (2018) have also explained that the isotherm 1/n value is an indication of surface site heterogeneity. The larger the 1/n value (smaller n value), the more heterogeneous the surface could be.

$$q_e = K_F c_e^{1/n} \tag{7}$$

Temkin. The Temkin isotherm (Eq. (8)) is a model that is physically based and effectively has two parameters in it—the Temkin isotherm constant related to the enthalpy of adsorption b_T [(J/mol)/(mg/g)], and the Temkin equilibrium binding constant K_T (L/mg) related to maximum binding energy (Shin and Kim, 2016). Other terms are the ideal gas constant R (8.314 J/mol-K) and temperature T (K). The Temkin isotherm is predicated on (a) the enthalpy of adsorption decreasing linearly with increase in fractional surface coverage and (b) adsorption is characterized by a uniform distribution of binding energies up to a maximum binding energy (Mall et al., 2005).

$$q_e = \frac{RT}{b_T} \ln \left(K_T c_e \right) \tag{8}$$

Dubinin-Radushkevich. The DR.. model (Eq. (9)) is a two-parameter empirical model that used the Polayni potential transformation of concentration ε (Eq. (10)) rather than concentration directly. Its parameters are the DR.. isotherm constant B (mol/J)², max adsorption capacity q_m (mg/g), ideal gas constant R (8.314 J/mol-K), and temperature T (K).

The model, though empirical, has a physical proposed mechanism of layer-by-layer coverage in pores leading to a pore-filling process. It is thus frequently used in microporous sorbents (Hutson and Yang, 1997).

$$q_e = q_m e^{-B\varepsilon^2} \tag{9}$$

$$\varepsilon = RT \ln \left(1 + \frac{1}{c_o} \right) \tag{10}$$

Sips. The Sips model (Eq. (11)) has also been called the Langmuir-Freundlich isotherm, and so it has the same parameters as each of those models. Because of the combination of the two models, the Sips isotherm is a three-parameter isotherm which has a Sips constant K_s [(mg/g)/(mg/L)^{1/n}] which operates as a combination of K_F and K_L , an affinity parameter n, and maximum adsorbed concentration q_m (mg/g). It has at times been an improvement over Freundlich and Langmuir models when adsorption is pH dependent (Inglezakis et al., 2018).

$$q_e = q_m \frac{K_S c_e^{1/n}}{1 + K_S c_e^{1/n}} \tag{11}$$

Krishnamurti. The Krishnamurti model (Eq. (12)) is also a three-parameter model based on adsorption reaction kinetics whereby the rate of adsorption is a second order equation based in the number of molecules left in solution and the amount that have currently adsorbed. Thus, the model conceives of higher rates of adsorption due to adsorbed molecules facilitating attachment of unadsorbed molecules (Chu, 2021). The parameters in the model are constant 1 k_1 (L/mg), constant 2 k_2 (unitless), and maximum adsorbed concentration (mg/g).

$$q_e = q_m \frac{1}{1 + k_2 e^{-k_1 c_e}} \tag{12}$$

3.2.3.4. Isotherm fit statistics. In addition to formulation of the models themselves, we selected a common set of model statistics to evaluate the models for goodness-of-fit. They are the coefficient of determination R^2 , the Root Mean Square Error (RMSE, Eq. (13)), the Relative Root Mean Square Error (RMSE, Eq. (14)), and the Average Relative Error (ARE, Eq. (15)). The terms in the equations are the total number of observations and predictions n, the modeled value \hat{q}_i , the true or experimental value q_i , and the number of model parameters p. The best model choice in the end was based primarily on the one with the lowest value RRMSE.

$$RMSE = \sqrt{\frac{\sum_{i=1}^{n} (\hat{q}_i - q_i)^2}{n}}$$
 (13)

$$RRMSE = \sqrt{\frac{\sum_{i=1}^{n} (\hat{q}_{i} - q_{i})^{2}}{n - p}}$$
 (14)

$$ARE = \frac{1}{n} \sum_{i=1}^{n} \left| \frac{\hat{q}_i - q_i}{q_i} \right|$$
 (15)

3.2.3.5. Isotherm model fits on experimental data. The individual model best fits with model fit statistics, identification of best-fit isotherm, and the parameters of the isotherm in the best are provided in Table 7. We fit the data using a numerical solver technique in Microsoft Excel whereby model parameters were varied until the RRMSE reached a minimum value. Once a visual fit of the model line confirmed a closeness to the data, we considered the isotherm model to be parameterized appropriately and ready for comparison to all of the other models for a biocharpHo-dye combination. We then put the best-fit model in the context of the experimental data and grouped the experiment data with model according to biomass and dye as shown in Fig. 12.

Crystal violet isotherms. First examining the CV data (upper two panels), it is seen that the adsorbed concentration is generally higher in CS biochar over PS biochar. Within the CS biochar, the initial shape of the

isotherm 0–50 mg/L is about the same for both TLUD and MF450 and at both pH $_{\rm o}$. It is the last point of the isotherm where we had to constrain each isotherm model to provide parameters that would fit all of the data with the least RRMSE. Most all of the conditions fit best with a concave down (Type I) isotherm (Langmuir or Freundlich). As well, all best fit isotherms indicate that a $q_{\rm m}$ (max adsorbed concentration) would exist with the exception being CS-MF450 pH $_{\rm o}$ 6, for which the Freundlich isotherm predicts that adsorption would continue ever higher as solution $c_{\rm e}$ increases.

In PS, the best models included the two three-parameter S-shaped isotherms (PS-MF450 pH $_{\rm o}$ 6, PS-TLUD pH $_{\rm o}$ 9). An RRMSE of about 1 mg/g q $_{\rm e}$ in each case indicates a high ability to predict adsorbed concentrations within the c $_{\rm e}$ range shown (0–450 mg/L CV). The other two datasets predicted Type I isotherms, which were both Freundlich. We also note that the PS-TLUD isotherms are very similar to one another showing low pH $_{\rm o}$ dependence. Their isotherm shapes are also almost the same even though different isotherm models are involved. Both the Sips and Freundlich models have an n adsorbate affinity parameter for which n > 1, which means that 1/n < 1. The result is that the solid partitioning of CV onto PS-TLUD biochar is fairly week, which is confirmed by the low maximum $q_{\rm e}$ shown in the data as 20 mg/g.

Methyl orange isotherms. The MO isotherms are in the bottom two panels. Looking at the data for CS, the spread in the data is fairly high indicating that the adsorption behavior is quantitatively distinct according to biochar type (TLUD, MF450) and pH $_{\!_{0}}$. The best-fit model for both pH $_{\!_{0}}$ 6 instances was a Sips S-shaped isotherm. The model predicted q_{m} was 28 and 43 mg/g for CS-MF450 and CS-TLUD, respectively. The CS-TLUD pH $_{\!_{0}}$ 9 isotherm is the only one that does not show a clear adsorption plateau in the data, and it is the only best-fit model for the Temkin isotherm. There is nothing in the Temkin isotherm model that constrains the adsorbate to have a maximum concentration. The CS-TLUD pH $_{\!_{0}}$ 9 isotherm for MO was the best adsorbing as previously discussed. It is possible that if still higher concentrations (lower BCD ratio) were used that it might level off.

In PS, the isotherms and the data themselves are much closer across all conditions. Yet there are subtle differences as indicated by the models that fit each one being different. We note in particular the PS-TLUD pH_o 9 KRM model, which shows the distinctive S-shape of a Type V isotherm. Looking closely at the data alone, this condition could be a Type IV isotherm as well. More investigation involved a greater number of points would confirm the type better. Within this set of isotherms, we also found that there was no clear leveling off leading to a max adsorbed concentration. The MF450 biochar at both pHo did have a model qm of 73 and 157 mg/g for pH_0 6 and 9, respectively. Compared to the MF450 in the CS then, the CS $q_{\rm m}$ was lower (20–30 mg/g) but was reached at much lower c_{ρ} than PS-MF450. In practice, this would indicate that CS-MF450 would not remove any additional MO at $c_e > 800$ mg/L. PS-MF450 on the other hand would remove more MO up until 90% of its q_m is reached which by the best fit models provided would be up to the reported solubility maximum of 5 g/L.

3.2.4. Comparison to other studies

We compared several other studies which have used methyl orange (MO) and crystal violet (CV) as dye test adsorptives. Rather than try to find similar biochar feedstock to what we used, we sought to examine differences between the work of others and ourselves using the same adsorptive as other studies.

3.2.4.6. Crystal violet. We looked in detail at the outcomes from other studies and summarized those findings in Table 8. It is difficult for us to make perfectly even comparisons because there are many ways to make biochar. As well, there is the potential for some researchers to use the study to optimize a biochar product for a particular purpose. In all studies shown, we selected the most strongly adsorbing biochar that an author used at the most favorable pH that they found. The work in our study is frequently distinct because, we did not seek to optimize

adsorption in any way. Rather, we examine a TLUD based biochar with common test dye adsorptives at pH values frequently found in natural waters (6–9). Since most studies reported at least Langmuir and Freundlich isotherm fits, we did the same to have an even comparison.

Most studies that we examined tried to fit their batch adsorption data to Freundlich and Langmuir isotherms. However, there were a few studies for CV that examined at least one other adsorption model (Wathukarage et al., 2019; Zubair et al., 2020). For these other studies, some of their best fitting isotherm models were models that we did not examine for our data, the Redlich-Peterson and Hill isotherms. Examining the model fit simply by the R^2 value, we find that our use of six different isotherm models allowed us to get a R^2 value that was frequently higher than other studies. Our fit may also be stronger due to the fact that we allowed for the use of a few three-parameter models whereas other authors only allowed for two-parameter models.

The performance of the TLUD biochars for cotton and pecan is lower for CV than for other studies examined, at least in terms of the maximum adsorbed concentration of CV (mg/g). Both of our maximum adsorption concentration were < 100 mg/g while other studies found concentrations well over 100 mg/g. The fact that the Freundlich capacity factor (K_f) is much lower in the TLUD (2.4, 3.9) biochars compared to the others (5.86–147) indicates that the greater adsorption for non-TLUD biochar should exist over the entire range of the isotherm.

The Freundlich n parameter is frequently called the adsorption intensity (Valsaraj, 2009), affinity (Clark, 2009), or energetic heterogeneity parameter (Worch, 2012). As ndecrease, the power law exponent 1/n increases. The effect of the larger 1/n value is to describe adsorption as being increasingly favorable at lower concentrations. Therefore, instances where Freundlich n values are lower have greater adsorption affinity. When the CV adsorption on biochar is compared in this way, the smallest n value (largest affinity) is the palm frond waste biochar of Zubair et al. (2020) at n = 1.41. The two TLUD biochars in our study have either lower or about the same n values (1.9 CS, 2.8 PS) as all of the other biochar selected from literature.

None of the biochar presented here from literature used any postpyrolysis treatment for activation behind grinding and washing, which is what we also have done. However, all of the studies used controlled heating rates in closed crucibles in a muffle furnace or under an inert gas atmosphere. Considering that we did not optimize the material in the TLUD in any way and had no controlled heating or slow pyrolysis, the adsorptive quality of the biochar for CV is reasonably high and comparable to lab-controlled biochar. Considering the MF biochar, which we created as a lab-style biochar, the TLUD biochar, using the same feedstock, adsorbs with about as much capacity and affinity.

3.2.4.7. Methyl orange. We present comparison MO studies in Table 9, and there is one major difference which most of them incorporated into their experimental design. Since these studies were frequently trying to optimize a biochar for a wastewater application, they optimized the initial pH of the MO solution to a more favorable MO adsorption.

Zhang et al. (2020) illustrates this process very clearly using a constant MO concentration solution adjusted to variations in pH units of 1.0 pH from 2.0–10.0 to ultimately find an optimum MO adsorption at pH 3.0 which they used for the rest of their study. Using pH of natural waters, the best adsorbing initial pH for MO was at the lower pH of 6.0. Authors consistently find that $pH \leq 4.0$ is best for MO adsorption. The reason for this finding is that MO is partially or completely protonated at lower pH due to its pK_a 3.47 value. The sulfonic acid functional group on the dye becomes neutral rather than negative, and the MO then has far less electrostatic repulsion between itself and negatively charged biochar surfaces. Considering then the context of our higher pH MO solutions against the lower pH solutions of many others, we should see lower adsorption capacity for MO on our biochar samples, which is what we found.

The maximum adsorbed concentration in TLUD biochar was < 50 mg/g generally compared to 80 mg/g or higher in literature. As

Table 8

Findings from other biochar studies involving crystal violet. In cases, where more study authors made more than one biochar and tested them for adsorption, we selected a single representative biochar. Biochar from this study is always the TLUD biochar at the most favorable pH. We present Isotherm values for biochar in our study only for Langmuir and Freundlich isotherms, even if they were not the best model fit, as many other studies use them. Thus, they better for purposes of comparison.

| study and biochar | isotherm findings | A_{BET} (m^2/g) | initial c_o (mg/L) and pH_o | max estimated q _e (mg/g) | representative isotherm values (T=25 °C) |
|--|---|---------------------|---------------------------------|-------------------------------------|---|
| Zubair et al. 2020: date palm fronds waste, pyrolyzed at temperature range 700 °C for 4 hr | Redlich-Peterson performed better than Langmuir and Freundlich (R^2 =0.934-0.975) | 432 | 20–200; 6.0 | 935 | Langmuir: q _m (mg/g) 935, K _L (L/mg) 0.66; Freundlich: K _f (mg/g)(L/mg) ^{1/n} 130, n 1.41 |
| Sewu et al., 2017a: Spent mushroom substrate and seaweed kelp, co-pyrolyzed at 500 °C for 60 min | Freundlich better than Langmuir for co-py BC (R^2 =0.812, 0.946) | 6.95 | 50-4000; 6.0 | 610 | Langmuir: q _m (mg/g) 610, K _L (L/mg) 0.011; Freundlich: K _f (mg/g)(L/mg) ^{1/n} 147, n 5.52 |
| Wathukarage et al. 2019: Woody tree Gliricidia sepium, pyrolyzed at 700 °C for 3 hr | Freundlich and Hill isotherms described data best out of several considered (R ² =0.975) | 808 | 5–200; 8.0 | 125 | Freundlich: K _f (mg/g)(L/mg) ^{1/n} 5.86, n 2.63 |
| This study: Cotton seed, pyrolyzed by TLUD | Langmuir, Krishnamurti best fits $(R^2=0.999-1.000)$ | 560 | 13–500; 9.0 | 61.1 | Langmuir: q _m (mg/g) 75.6, K _L (L/mg) 0.0219; Freundlich: K _f (mg/g)(L/mg) ^{1/n} 3.91, n 1.9 |
| Pecan shell, pyrolyzed by TLUD | Sips and Freundlich isotherms provide best fits (R^2 =0.986-0.991) | 430 | 13–500; 9.0 | 30.6 | Langmuir: q _m (mg/g) 21.3, K _L (L/mg) 0.0244; Freundlich: K _f (mg/g)(L/mg) ^{1/n} 2.41, n 2.8 |

Table 9
Findings from other biochar studies involving methyl orange. In cases, where more study authors made more than one biochar and tested them for adsorption, we selected a single representative biochar. Biochar from this study is always the TLUD biochar at the most favorable pH. We present Isotherm values for biochar in our study only for Langmuir and Freundlich isotherms, even if they were not the best model fit, as many other studies use them. Thus, they better for purposes of

| Study and biochar | isotherm findings | A_{BET} (m^2/g) | initial c_o (mg/L) and pH_o | q _e (mg/g) | Representative isotherm values |
|--|---|---------------------|-----------------------------------|-----------------------|--|
| Wang et al. 2016: wheat straw pyrolyzed at 450 °C, washed in KOH (m _{KOH} :m _{bc} =4), further pyrolyzed at 700 °C, followed by final wash in HCl and DI | Langmuir adsorption fit slightly better than Freundlich (R ² =1.000) | 2263 | 400-1200; 6.8-7.2 (natural pH) | 1109 | Langmuir: q _m (mg/g) 1109, K _L (L/mg) 0.0381; Freundlich: K _f (mg/g)(L/mg) ^{1/n} 452, n 10.05 |
| Zhang et al. 2020: pomelo peel waste, pre-washed in 85% H ₃ PO ₄ , then pyrolyzed at 450 °C for 60 min | Freundlich isotherm more favorable than Langmuir, Temkin, BET (R ² =0.986) | 75.3 | 30–150; 3.0 | 148 | Langmuir: $q_m(mg/g)$ 163, K_L (L/mg) 2.92; Freundlich: K_f (mg/g)(L/mg) ^{1/n} 113, n 2.69 |
| Zubair et al. 2020: date palm fronds waste, pyrolyzed at temperature range 500-800 °C for 2-4 hr | Langmuir performed better than Redlich-Peterson and Freundlich (R ² =0.984) | 432 | 20–200; 4.0 | 163 | Langmuir: $q_m(mg/g)$ 163, K_L (L/mg) 0.008; Freundlich: $K_f (mg/g)(L/mg)^{1/n}$ 27.6, n 4.17 |
| Kaya and Uzun 2020 (Kaya and Uzun): Pine cones, pyrolyzed at 600 °C, washed in KOH at 800 °C for 1 hr, then neutralized with HCl | Freundlich performed better than Langmuir $(R^2=0.982)$ | 1715 | 100-400; 2.0 | 80.4 | Langmuir: $q_m(mg/g) 80.4$, K_L (L/mg) 0.261; Freundlich: $K_f (mg/g)(L/mg)^{1/n}$ 20.2, n 0.421 |
| This study: Cotton seed, pyrolyzed by TLUD | Sips and Temkin best fit $(R^2=0.981)$ | 560 | 33–1500; 6.0 | 42.5 | Langmuir: $q_m(mg/g)$ 54.8, K_L (L/mg) 0.00637; Freundlich: $K_f (mg/g)(L/mg)^{1/n}$ 2.51, n 2.3 |
| This study: Pecan shell, pyrolyzed by TLUD | Sips and Langmuir best fit (R ² =0.958, 0.961) | 430 | 33–1500; 6.0 | 49.7 | Langmuir: $q_m(mg/g)$ 109,000, K_L (L/mg) 3.27 × 10 ⁻⁷ Freundlich: K_f (mg/g)(L/mg) ^{1/n} 0.0226, n 0.94 |

well, the biochar in many of the comparison studies not only used a lower pH but also activation or multi-stage pyrolysis to further optimize their biochar. Using the $\rm K_f$ as a general measure of adsorption capacity, the TLUD biochar was lower in overall capacity by 10-20,000x depending on the TLUD biochar compared. In contrast, the $\it n$ Freundlich affinity parameter of our TLUD biochar was as low as or lower than many of the lab-produced biochars from literature. The biggest different in all feedstock-dye combinations for our own lab-produced versus TLUD biochar was for MO on CS. The data provided in Fig. 12 shows a much greater adsorption capacity for TLUD biochar compared to MF. The TLUD device we expect gets much hotter than the 450 °C use in our MF biochar, and this may be one of the reasons for this difference.

The overall surface area for the TLUD biochar is still fairly high at $\geq 400 {\rm m}^2/{\rm g}$. This high surface area, especially compared to the minimal surface area of the original feedstock, combined with reasonable adsorptive ability of the TLUD biochar at a pH of 6.0 suggests that the adsorptive characteristics of a TLUD biochar for an anionic pollutant are promising.

3.2.5. Mechanistic considerations for adsorption according to biochar production method

Given the generally inconsistent effects of adsorptive uptake between dye and biochar combination in our data, it difficult to provide a single mechanistic explanation for what we see. Nonetheless, what follows are some possibilities supported in the data.

We examined literature to see what others have found with respect to cationic and anionic adsorption that could help to explain the behavior between MF450 and TLUD biochar. Regarding pH, we see that it matters in many situations because of biochar surface charge state (if $pH > pH_{zpc}$, then the surface is net negative and vice versa) and the state of the adsorbate according to pH. As many dyes are ionizable according to pH, then the adsorptive potential of a cation or anion exchange site on the biochar surface depends on whether or not the adsorbate exists in ionic form or not. Both dyes we used had pKa < pH of initial solution pH. Many biochar when placed in water tend to raise rather than lower pH presumably due to ash content (Al-Wabel et al., 2013), and this is what we saw from spot measurements of post adsorption solutions. Thus, the anionic and cationic dyes should exist in deprotonated forms in all our experiments meaning that they will remain as singly charged (±1) ions. The biochar, on the other hand, may have experienced significant surface charge alteration at the initial pH we examined (6, 9) as evidenced by others who reported pH_{zpc} ranging 6-11 (Caglar et al., 2018; Vyavahare et al., 2019; Wathukarage et al., 2019; Yang et al., 2015b; Zubair et al., 2020). For our study, we only saw a noticeable pH shift in adsorption for MO on cotton seed biochar. We thus suggest that the CS- MF450 biochar likely has a lower pH_{zpc} than the CS-TLUD biochar. That this effect in CS only occurs in MO hints that the adsorption mechanism for MO is strongly related to the number and availability of anionic exchange sites on the surface. Others (He et al., 2020; Zhang et al., 2020; Zubair et al., 2020) have noted that methyl orange dyes exhibited Langmuir monolayer adsorption behavior on many biochar types whereas crystal violet allowed a cooperative multilayer adsorption to occur (Wathukarage et al., 2019; Zubair et al., 2020) . Our data are generally consistent with this possibility since MO adsorption seems more limited than CV.

Looking at material differences, we saw in TLUD vs MF450 biochar, two of the biggest were the higher specific surface area and the increased ash content in TLUD biochar (especially for PS). We see adsorption mechanisms in these trends as well. Considering surface area, higher pyrolysis temperature leads to higher surface area and to higher aromatic character generally (Al-Wabel et al., 2013; Hung et al., 2017; Kang et al., 2018; Smebye et al., 2016). For dyes, others (Wang et al., 2016; Wathukarage et al., 2019; Zubair et al., 2020) have noted the importance of pi-pi bonding in both MO and CV. The fact that the CS-TLUD biochar (having higher degree of pyrolysis) adsorbs MO more strongly than the CS-MF450 supports this pi-pi bond mechanism as being consequential for MO. Seeing as how lower surface area (and presumably lower aromatic character) PS-MF450 adsorbs CV more strongly than PS-TLUD, we suggest that any effect of increased pi-pi bonding for CV is overcome by the increased number of negatively charged functional groups on MF450. Ash content has been shown (Sewu et al., 2017b; Yang et al., 2015b) to result in increased adsorption for positively charged compounds. The reason given for this trend is that alkali and earth alkali metals (Ca²⁺, Mg²⁺, K⁺) can be released and exchanged for those compounds. The increased ash content, being higher in both CS and PS TLUD biochar, did not result in any increase in adsorption for crystal violet as might be expected from ash-based cationic exchange locations. The lack of effect in this way suggests again that the organic functional groups, which were higher in the MF450 biochar, were more influential for strength of adsorption than adsorption connected to inorganic sites.

4. Discussion

With all of the individual material and adsorption-based measurements described, it is valuable to provide a summary interpretation of why the cation and anionic test adsorptives behave as they do. We provide a detailed summary table all of the individual analysis findings in the SI. Here we report the interpretation from that summary.

Material results. The differences in biochar are dependent on both production conditions as well as original feedstock. The PS had more

lignin than the CS, and this difference made it such that materially the methods of production made a more different biochar in PS compared to CS. The TLUD method we used clearly results in a higher maximum pyrolysis temperature than the MF450. The higher temperature for TLUD led to a lower quantity of surface functional groups, higher specific surface area, smaller pore sizes, lower production yield, higher ash content, greater carbonization, and lower residual cellulose crystallinity. Because the PS has more lignin compared to CS and lignin is more thermally stable, all of the differences related to production method mattered more in PS over CS. Thus, the starting material would matter a great deal in the overall quality of biochar using developing world production methods.

Many developing world production methods are similar to the TLUD in that they use a flame as a heat source, have uneven heating, use no controlled temperature ramping, are manually monitored, and have some oxygen present. Given these commonalities in many simple biochar production methods, we would suppose that the more lignin is present in the original feedstock, the more variation there can be in the final biochar and the more refinement in developing world production methods would do for a particular biochar application. Most low-resource contexts cannot easily choose what crop waste residue they have on hand in abundant qualities. The TLUD style biochar production method may not always be the best according to the use of the biochar and readily available feedstock. However, nearly all low-resource production methods have some means to alter production conditions (such as time, manual stirring, level of flame, air damping) and thus could be adjusted according to the final biochar desired.

Environmental performance. We only looked at cationic and anionic dyes in our testing. These model pollutants are similar at least in their charged nature to dissolved metals, nutrients, and organics with ionizable groups. Our model compounds cannot speak as directly to hydrophobic micropollutants. With these caveats in mind, we still find that biochar made in the TLUD was a reasonable high quality biochar. It did remove these dyes at concentrations, which were of environmental relevance (< 100 mg/L) frequently at levels > 50% of dissolved dye. We also saw that the performance of the TLUD biochar made by highly uncontrolled pyrolysis was similar to the lab-controlled biochar made in a muffle furnace.

For MO, we can tell that both the MF450 and TLUD biochar were not terribly effective at pollutant removal though we still saw quantifiable removal. The reason for the poorer removal was at least in part due to our not optimizing pH for MO. Other authors found that a pH lower and closer to the pKa of MO created better removal due to increased protonation of the compound. So performance of DWB could be enhanced for removing some pollutants if pH were much lower. However, the challenge for environmental performance and understanding what it might be in developing world setting depends very much on the exact application. If the desire for the biochar is to remove residual agrochemicals from soil water or agricultural runoff, then what we have seen in our TLUD biochar would indicate that this purpose will often be facilitated.

If the desire for DWB were more as a nutrient repository, then it is likely that bioavailable nutrients, native in the biochar ash content will provide them. It is not as clear what the nutrient related benefits will be for TLUD biochar after the native nutrients are exhausted. It may be that cationic and anionic nutrients will behave similarly to CV and MO and that they will adsorb and release as needed by crops, grasses, and wild plants. Many complications beyond the scope of our study (TDS, DOM, competitive adsorption, aging) would need to be investigated in a field or greenhouse setting to know.

If the desire for the DWB were to treat wastewater or improve a drinking water source, we see potential for this as well. The overall specific surface areas we find in the TLUD biochars are not as high as an activated carbon, but they may not need to be. These models dyes were still removed at appreciable levels. The interest in DWBs of the kind we have made is that they are not terribly difficult to make and do not require additional costly activation steps or precise control technologies.

It may be that the techno-economic balance between cost, performance, and local context could justify a TLUD or similar biochar for a wastewater or drinking water application.

5. Conclusions

In this study, we examined the use of a developing world style biochar (DWB) production method, the top-lit updraft (TLUD), against a lab-controlled muffle furnace created biochar using common crop waste residue, pecan shell and cottonseed. We examined the biochar created in terms of material properties and in water spiked with anionic and cationic dyes to understand environmental performance. We found that the differences in production method matter more for the PS over the CS because PS has higher lignin content while CS show signs of higher cellulose. Lignin does not lose as much mass overall as hemicellulose or cellulose and can thus generate high yield, microporous biochar. The TLUD method generally reached higher temperatures due the uncontrolled nature of the pyrolysis resulting in a more carbonized biochar. The resultant environmental performance of the TLUD-based biochars was comparable to lab-based biochars for the dyes we used. As well, we find that the adsorption potential of TLUD biochar, though less than biochars found in literature, was nonetheless effective.

We would recommend that future studies in DWB examine other aspects of its behavior that we did not get to examine. These aspects would include comparisons of different simple biochar production methods beyond the TLUD, investigate DWB at the field scale (in case of ag use) or full scale (in case of large community water treatment), and perform techno-economic analysis whereby the cost to produce biochar is balanced against the value that it provides. We think that future research efforts should link what is known about the properties and behavior in lab-optimized biochar with low-resource setting biochar. We hypothesize that synergy between these two biochar applications arenas would be mutually beneficial.

Declaration of Competing Interest

We declare no competing interests in this work.

Acknowledgements

Authors would like to acknowledge the financial support of the Kilgore Faculty Research program at West Texas A&M University. We also acknowledge Micromeritics Analytical Services for providing us complimentary, free-of-charge surface characterization of biochar. We thank Colin Voiles for designing and optimizing the original TLUD biochar device we used. Finally, we thanks two anonymous reviewers for their helpful suggestions to improve the manuscript.

References

- Ahmad, M., Rajapaksha, A.U., Lim, J.E., Zhang, M., Bolan, N., Mohan, D., Vithanage, M., Lee, S.S., Ok, Y.S., 2014. Biochar as a sorbent for contaminant management in soil and water: a review. Chemosphere 99, 19–33.
- Al-Wabel, M.I., Al-Omran, A., El-Naggar, A.H., Nadeem, M., Usman, A.R.A., 2013. Pyrolysis temperature induced changes in characteristics and chemical composition of biochar produced from conocarpus wastes. Bioresour. Technol. 131, 374–379.
- Alexandratos, N., Bruinsma, J., 2012. World Agriculture Towards 2030/2050: the 2012 Revision. Food and Agriculture Organization of the United Nations (FAO), Rome.
- An, L., Deng, J., Zhou, L., Li, H., Chen, F., Wang, H., Liu, Y., 2010. Simultaneous spectrophotometric determination of trace amount of malachite green and crystal violet in water after cloud point extraction using partial least squares regression. J. Hazard. Mater. 175, 883–888.
- Atalla, R.H., VanderHart, D.L., 1984. Native cellulose: a composite of two distinct crystalline forms. Science 223, 283–285.
- Ayawei, N., Ebelegi, A.N., Wankasi, D., 2017. Modelling and interpretation of adsorption isotherms. J. Chem. 2017. 3039817.
- Azami, M., Bahram, M., Nouri, S., Naseri, A., 2012. A central composite design for the optimization of the removal of the azo dye, Methyl Orange, from waste water using the Fenton reaction. J. Serbian Chem. Soc. 77, 235–246.
- Bayabil, H.K., Stoof, C.R., Lehmann, J.C., Yitaferu, B., Steenhuis, T.S., 2015. Assessing the potential of biochar and charcoal to improve soil hydraulic properties in the humid Ethiopian Highlands: the Anjeni watershed. Geoderma 243, 115–123.

- Bhadha, J.H., Jennewein, S., Sanchez, J., Lang, T.A., 2021. Producing Biochar Using a Custom Designed Top-Lit Updraft (Tlud) Gasifier 1.
- Birzer, C., Medwell, P., MacFarlane, G., Read, M., Wilkey, J., Higgins, M., West, T., 2014.

 A biochar-producing, dung-burning cookstove for humanitarian purposes. Procedia Eng. 78, 243–249.
- Blayney, D., Gutierrez, P., 2017. NMSU: Economic Importance of the Pecan Industry. New Mexico State University (NMSU), Las Cruces.
- Brewer, C.E., Hall, E.T., Schmidt-Rohr, K., Laird, D.A., Brown, R.C., Zygourakis, K., 2017.
 Temperature and reaction atmosphere effects on the properties of corn stover biochar.
 Environ. Prog. Sustain. Energy 36, 696–707.
- Brookes, G., Barfoot, P., 2018. Farm income and production impacts of using GM crop technology 1996–2016. GM Crops Food 9, 59–89.
- Caglar, E., Donar, Y.O., Sinag, A., Birogul, I., Bilge, S., Aydincak, K., Pliekhov, O., 2018. Adsorption of anionic and cationic dyes on biochars, produced by hydrothermal carbonization of waste biomass: effect of surface functionalization and ionic strength. Turk. J. Chem. 42 86-+.
- Cao, X.D., Ma, L.N., Gao, B., Harris, W., 2009. Dairy-manure derived biochar effectively sorbs lead and atrazine. Environ. Sci. Technol. 43, 3285–3291.
- Cely, P., Gasco, G., Paz-Ferreiro, J., Mendez, A., 2015. Agronomic properties of biochars from different manure wastes. J. Anal. Appl. Pyrolysis 111, 173–182.
- Chu, K.H., 2021. Fitting a little-known isotherm equation to S-shaped adsorption equilibrium data. Sep. Purif. Technol. 259, 118079.
- Clark, M.M., 2009. Transport Modeling For Environmental Engineers and Scientists, Second ed. Wiley, Hoboken, NJ, USA.
- Dada, A.O., Olalekan, A., Olatunya, A., Dada, A.O., 2012. Langmuir, Freundlich, Temkin and Dubinin–Radushkevich Isotherms Studies of Equilibrium Sorption of Zn 2+ Unto Phosphoric Acid Modified Rice Husk. J. Appl. Chem. 3, 38–45.
- de la Rosa, J.M., Rosado, M., Paneque, M., Miller, A.Z., Knicker, H., 2018. Effects of aging under field conditions on biochar structure and composition: implications for biochar stability in soils. Sci. Total Environ. 613, 969–976.
- Deng, L., Torres-Rojas, D., Burford, M., Whitlow, T.H., Lehmann, J., Fisher, E.M., 2018. Fuel sensitivity of biomass cookstove performance. Appl. Energy 215, 13–20.
- Fan, S.S., Wang, Y., Wang, Z., Tang, J., Tang, J., Li, X.D., 2017. Removal of methylene blue from aqueous solution by sewage sludge-derived biochar: adsorption kinetics, equilibrium, thermodynamics and mechanism. J. Environ. Chem. Eng. 5, 601–611.
- FAO, 2002. World agriculture: Towards 2015:2030, Summary Report. Food and Agriculture Organization of the United Nations, Rome.
- G, R., Singh, B., 2013. Cellulose crystallinity change assessment of biochar produced by pyrolysis of coir pith. Res. J. Recent Sci. 2, 2277–2502.
- Gai, X.P., Wang, H.Y., Liu, J., Zhai, L.M., Liu, S., Ren, T.Z., Liu, H.B., 2014. Effects of feedstock and pyrolysis temperature on biochar adsorption of ammonium and nitrate. PLoS One 9, 19.
- Gonzaga, M.I.S., Mackowiak, C.L., Comerford, N.B., Moline, E.F.D., Shirley, J.P., Guimaraes, D.V., 2017. Pyrolysis methods impact biosolids-derived biochar composition, maize growth and nutrition. Soil Tillage Res. 165, 59–65.
- Gwenzi, W., Chaukura, N., Mukome, F.N.D., Machado, S., Nyamasoka, B., 2015. Biochar production and applications in sub-Saharan Africa: opportunities, constraints, risks and uncertainties. J. Environ. Manag. 150, 250–261.
- Han, L., Xue, S., Zhao, S., Yan, J., Qian, L., Chen, M., 2015. Biochar supported nanoscale iron particles for the efficient removal of methyl orange dye in aqueous solutions. PLoS One 10, 1–15.
- He, C., Lin, H.L., Dai, L.L., Qiu, R.L., Tang, Y.T., Wang, Y.P., Duan, P.G., Ok, Y.S., 2020. Waste shrimp shell-derived hydrochar as an emergent material for methyl orange removal in aqueous solutions. Environ. Int. 134.
- Herbert, L., Hosek, I., Kripalani, R., Vanasupa, L., 2012. The characterization and comparison of biochar produced from a decentralized reactor using forced air and natural draft pyrolysis.
- Huang, C.F., Stein, H.H., Zhang, L.Y., Li, D., Lai, C.H., 2017. Concentrations of minerals in pig feed ingredients commonly used in China. Transl. Anim. Sci. 1, 126–136.
- Hung, C.Y., Tsai, W.T., Chen, J.W., Lin, Y.Q., Chang, Y.M., 2017. Characterization of biochar prepared from biogas digestate. Waste Manag. 66, 53–60.
- Hutson, N.D., Yang, R.T., 1997. Theoretical basis for the Dubinin-Radushkevitch (D-R) adsorption isotherm equation. Adsorption 3, 189–195.
- Inglezakis, V.J., Poulopoulos, S.G., Kazemian, H., 2018. Insights into the S-shaped sorption isotherms and their dimensionless forms. Microporous Mesoporous Mater. 272, 166–176.
- James, R.A.M., Yuan, W., Boyette, M.D., 2016. The effect of biomass physical properties on top-lit updraft gasification of woodchips. Energies 9.
- Janczak, D., Malinska, K., Czekala, W., Caceres, R., Lewicki, A., Dach, J., 2017. Biochar to reduce ammonia emissions in gaseous and liquid phase during composting of poultry manure with wheat straw. Waste Manag. 66, 36–45.
- Jasiukaityte-Grojzdek, E., Kunaver, M., Poljanšek, I., 2012. Influence of cellulose polymerization degree and crystallinity on kinetics of cellulose degradation. BioResources.
- Johar, N., Ahmad, I., Dufresne, A., 2012a. Extraction, preparation and characterization of cellulose fibres and nanocrystals from rice husk. Ind. Crops Prod. 37, 93–99.
- Johar, N., Ahmad, I., Dufresne, A., 2012b. Extraction, preparation and characterization of cellulose fibres and nanocrystals from rice husk. Ind. Crops Prod.
- Kang, C.L., Zhu, L., Wang, Y.X., Wang, Y.H., Xiao, K.K., Tian, T., 2018. Adsorption of basic dyes using walnut shell-based biochar produced by hydrothermal carbonization. Chem. Res. Chin. Univ. 34, 622–627.
- Kaya, N., Uzun, Z.Y., 2020. Investigation of effectiveness of pine cone biochar activated with KOH for methyl orange adsorption and ${\rm CO_2}$ capture. Biomass Convers. Biorefinery.
- Kearns, J., 2012. Sustainable decentralized water treatment for rural developing communities using locally generated biochar adsorbents. Water Cond. Purif. Mag..

- Langford, J.I., Wilson, A.J.C., 1978. Scherrer after sixty years: A survey and some new results in the determination of crystallite size. J. Appl. Crystallogr..
- Lee, J.W., Kidder, M., Evans, B.R., Paik, S., Buchanan, A.C., Garten, C.T., Brown, R.C., 2010. Characterization of biochars produced from cornstovers for soil amendment. Environ. Sci. Technol. 44, 7970–7974.
- Lehmann, J., Joseph, S., 2015. Biochar For Environmental Management: Science and Technology, second ed. Earthscan.
- Li, S.M., Harris, S., Anandhi, A., Chen, G., 2019. Predicting biochar properties and functions based on feedstock and pyrolysis temperature: a review and data syntheses. J. Clean. Prod. 215, 890–902.
- Li, Z., Chen, K., Chen, Z., Li, W.N., Biney, B.W., Guo, A.J., Liu, D., 2021. Removal of malachite green dye from aqueous solution by adsorbents derived from polyurethane plastic waste. J. Environ. Chem. Eng. 9.
- Liu, X., Sun, J., Duan, S., Wang, Y., Hayat, T., Alsaedi, A., Wang, C., Li, J., 2017. A valuable biochar from poplar catkins with high adsorption capacity for both organic pollutants and inorganic heavy metal ions. Sci. Rep..
- Lohri, C.R., Rajabu, H.M., Sweeney, D.J., Zurbrugg, C., 2016. Char fuel production in developing countries – a review of urban biowaste carbonization. Renew. Sustain. Energy Rev. 59, 1514–1530.
- Maican, E., Dutu, I.C., Matache, G., Dumitrescu, C., Pavel, I., 2017. CFD analysis of an improved tlud based equipment for heating small greenhouses and hothouses. Inmateh-Agric. Eng. 53, 5–12.
- Mall, I.D., Srivastava, V.C., Agarwal, N.K., Mishra, I.M., 2005. Removal of congo red from aqueous solution by bagasse fly ash and activated carbon: Kinetic study and equilibrium isotherm analyses. Chemosphere 61, 492–501.
- Mandal, A., Singh, N., Purakayastha, T.J., 2017. Characterization of pesticide sorption behaviour of slow pyrolysis biochars as low cost adsorbent for atrazine and imidacloprid removal. Sci. Total Environ. 577, 376–385.
- Masis-Melendez, F., Segura-Chavarria, D., Garcia-Gonzalez, C.A., Quesada-Kimsey, J., Villagra-Mendoza, K., 2020. Variability of physical and chemical properties of TLUD stove derived biochars. Appl. Sci. 10.
- Mendez, A., Gomez, A., Paz-Ferreiro, J., Gasco, G., 2012. Effects of sewage sludge biochar on plant metal availability after application to a Mediterranean soil. Chemosphere 89, 1354–1359.
- Meng, J., Wang, L.L., Liu, X.M., Wu, J.J., Brookes, P.C., Xu, J.M., 2013. Physicochemical properties of biochar produced from aerobically composted swine manure and its potential use as an environmental amendment. Bioresour. Technol. 142, 641–646.
- Nam, S., French, A.D., Condon, B.D., Concha, M., 2016. Segal crystallinity index revisited by the simulation of X-ray diffraction patterns of cotton cellulose I β and cellulose II. Carbohydr. Polym.
- Nansubuga, I., Banadda, N., Ronsse, F., Verstraete, W., Rabaey, K., 2015. Digestion of high rate activated sludge coupled to biochar formation for soil improvement in the tropics. Water Res. 81, 216–222.
- Noori, A., Bartoli, M., Frache, A., Piatti, E., Giorcelli, M., Tagliaferro, A., 2020. Development of pressure-responsive polypropylene and biochar-based materials. Micromachines 11.
- Novak, J.M., Cantrell, K.B., Watts, D.W., Busscher, W.J., Johnson, M.G., 2014. Designing relevant biochars as soil amendments using lignocellulosic-based and manure-based feedstocks. J. Soils Sediments 14, 330–343.
- Pandit, N.R., Mulder, J., Hale, S.E., Schmidt, H.P., Cornelissen, G., 2017. Biochar from "Kon Tiki" flame curtain and other kilns: effects of nutrient enrichment and kiln type on crop yield and soil chemistry. PLoS One 12.
- Paneque, M., De la Rosa, J.M., Franco-Navarro, J.D., Colmenero-Flores, J.M., Knicker, H., 2016. Effect of biochar amendment on morphology, productivity and water relations of sunflower plants under non-irrigation conditions. Catena 147, 280–287.
- Peng, C., Feng, W., Zhang, Y.H., Guo, S.F., Yang, Z.L., Liu, X.M., Wang, T.F., Zhai, Y.B., 2021. Low temperature co-pyrolysis of food waste with PVC-derived char: Products distributions, char properties and mechanism of bio-oil upgrading. Energy 219.
- Peterson, S.C., Jackson, M.A., 2014. Simplifying pyrolysis: using gasification to produce corn stover and wheat straw biochar for sorptive and horticultural media. Ind. Crops Prod. 53, 228–235.
- Rajapaksha, A.U., Chen, S.S., Tsang, D.C.W., Zhang, M., Vithanage, M., Mandal, S., Gao, B., Bolan, N.S., Ok, Y.S., 2016. Engineered/designer biochar for contaminant removal/immobilization from soil and water: potential and implication of biochar modification. Chemosphere 148, 276–291.
- Rajendran, S., Veerasimman, A., Vairavan, M., Shanmugam, V., Rajendran, D.J.J., 2020. Mechanical performance studies on composites using polyethylene terephthalate char derived from polyethylene terephthalate waste bottle-reinforced polyester composites. Mater. Perform. Charact. 9, 726–738.
- Ro, K.S., Hunt, P.G., Jackson, M.A., Compton, D.L., Yates, S.R., Cantrell, K., Chang, S.C., 2014. Co-pyrolysis of swine manure with agricultural plastic waste: Laboratory-scale study. Waste Manag. 34, 1520–1528.

- Rojith, G., Singh, B., 2013. Cellulose crystallinity change assessment of biochar produced by pyrolysis of coir pith. Res. J. Recent Sci. 2, 2277–2502.
- Sajdak, M., Muzyka, R., Hrabak, J., Slowik, K., 2015. Use of plastic waste as a fuel in the co-pyrolysis of biomass Part III: optimisation of the co-pyrolysis process. J. Anal. Appl. Pyrolysis 112, 298–305.
- Sewu, D.D., Boakye, P., Jung, H., Woo, S.H., 2017a. Synergistic dye adsorption by biochar from co-pyrolysis of spent mushroom substrate and Saccharina japonica. Bioresour. Technol. 244, 1142–1149.
- Sewu, D.D., Boakye, P., Woo, S.H., 2017b. Highly efficient adsorption of cationic dye by biochar produced with Korean cabbage waste. Bioresour. Technol. 224, 206–213.
- Shin, H.S., Kim, J.-H., 2016. Isotherm, kinetic and thermodynamic characteristics of adsorption of paclitaxel onto Diaion HP-20. Process Biochem. 51, 917–924.
- Smebye, A., Ailing, V., Vogt, R.D., Gadmar, T.C., Mulder, J., Cornelissen, G., Hale, S.E., 2016. Biochar amendment to soil changes dissolved organic matter content and composition. Chemosphere 142, 100–105.
- Song, X., Sun, L.N., Li, K., Sun, X., Wang, C., Ning, P., 2019. Influence of surface characteristics on carbon disulfide catalytic hydrolysis over modified lake sediment biochar and research on deactivated mechanism. Surf. Interface Anal. 51, 1093–1101.
- Sparrevik, M., Field, J.L., Martinsen, V., Breedveld, G.D., Cornelissen, G., 2013. Life cycle assessment to evaluate the environmental impact of biochar implementation in conservation agriculture in Zambia. Environ. Sci. Technol. 47, 1206–1215.
- Tryner, J., Willson, B.D., Marchese, A.J., 2014. The effects of fuel type and stove design on emissions and efficiency of natural-draft semi-gasifier biomass cookstoves. Energy Sustain. Dev. 23, 99–109.
- Uzoma, K.C., Inoue, M., Andry, H., Fujimaki, H., Zahoor, A., Nishihara, E., 2011. Effect of cow manure biochar on maize productivity under sandy soil condition. Soil Use Manag. 27, 205–212.
- Valsaraj, K.T., 2009. Elements of Environmental Engineering, third ed. CRC Press, Boca Raton.
- Vyavahare, G., Jadhav, P., Jadhav, J., Patil, R., Aware, C., Patil, D., Gophane, A., Yang, Y.H., Gurav, R., 2019. Strategies for crystal violet dye sorption on biochar derived from mango leaves and evaluation of residual dye toxicity. J. Clean. Prod. 207, 296–305.
- Wang, P.F., Wu, C.F., Guo, Y., Wang, C., 2016. Experimental and theoretical studies on methylene blue and methyl orange sorption by wheat straw-derived biochar with a large surface area. PCCP 18, 30196–30203.
- Wathukarage, A., Herath, I., Iqbal, M.C.M., Vithanage, M., 2019. Mechanistic understanding of crystal violet dye sorption by woody biochar: implications for wastewater treatment. Environ. Geochem. Health 41, 1647–1661.
- Worch, E., 2012. Adsorption Technology in Water Treatment Berlin.
- Xie, T., Reddy, K.R., Wang, C.W., Yargicoglu, E., Spokas, K., 2015. Characteristics and applications of biochar for environmental remediation: a review. Crit. Rev. Environ. Sci. Technol. 45, 939–969.
- Xu, Y., Deng, F.F., Pang, Q.C., He, S.W., Xu, Y.Q., Luo, G.Q., Yao, H., 2018. Development of waste-derived sorbents from biomass and brominated flame retarded plastic for elemental mercury removal from coal-fired flue gas. Chem. Eng. J. 350, 911–919.
- Xue, Y., Zhou, S., Brown, R.C., Kelkar, A., Bai, X.L., 2015. Fast pyrolysis of biomass and waste plastic in a fluidized bed reactor. Fuel 156, 40–46.
- Yang, G., Wang, Z., Xian, Q., Shen, F., Sun, C., Zhang, Y., Wu, J., 2015a. Effects of pyrolysis temperature on the physicochemical properties of biochar derived from vermicompost and its potential use as an environmental amendment. RSC Adv. 5, 40117–40125.
- Yang, G., Wang, Z.H., Xian, Q.M., Shen, F., Sun, C., Zhang, Y.Z., Wu, J., 2015b. Effects of pyrolysis temperature on the physicochemical properties of biochar derived from vermicompost and its potential use as an environmental amendment. RSC Adv. 5, 40117–40125.
- Yang, H.P., Yan, R., Chen, H.P., Zheng, C.G., Lee, D.H., Liang, D.T., 2006. In-depth investigation of biomass pyrolysis based on three major components: hemicellulose, cellulose and lignin. Energy Fuels 20, 388–393.
- Yu, P.W., Xue, Y.W., Gao, F., Liu, Z.G., Cheng, X.R., Yang, K., 2016. Phosphorus removal from aqueous solution by pre- or post-modified biochars derived from agricultural residues. Water Air Soil Pollut. 227. 9.
- Yuan, J.H., Xu, R.K., 2011. The amelioration effects of low temperature biochar generated from nine crop residues on an acidic Ultisol. Soil Use Manag. 27, 110–115.
- Zhang, B., Wu, Y.H., Cha, L.G., 2020. Removal of methyl orange dye using activated biochar derived from pomelo peel wastes: performance, isotherm, and kinetic studies. J. Dispers. Sci. Technol. 41, 125–136.
- Zhang, Y.H., Idowu, O.J., Brewer, C.E., 2016. Using agricultural residue biochar to improve soil quality of desert soils. Agriculture 6.
- Zubair, M., Mu¹azu, N.D., Jarrah, N., Blaisi, N.I., Aziz, H.A., Al-Harthi, M.A., 2020. Adsorption behavior and mechanism of methylene blue, crystal violet, Eriochrome Black T, and methyl orange dyes onto biochar-derived date palm fronds waste produced at different pyrolysis conditions. Water Air Soil Pollut. 231.